ANL-7082

ANL-7082

Argonne National Laboratory

REACTOR DEVELOPMENT PROGRAM

PROGRESS REPORT

July 1965

DISCLAIMER

LEGAL NOTICE

Printed in USA. Price $3.00. Available from the Clearinghouse for Federal Scientific and Technical Information, National Bureau of Standards, U. S. Department of Commerce, Springfield, Virginia

ANL-7082
Reactor Technology
(TID-4500, 43rd Ed.)
AEC Research and
Development Report

ARGONNE NATIONAL LABORATORY
9700 South Cass Avenue
Argonne, Illinois 60440

REACTOR DEVELOPMENT PROGRAM PROGRESS REPORT

July 1965

Albert V. Crewe, Laboratory Director
Stephen Lawroski, Associate Laboratory Director

Division	Director
Chemical Engineering	R. C. Vogel
Idaho	M. Novick
Metallurgy	F. G. Foote
Reactor Engineering	L. J. Koch
Reactor Physics	R. Avery
Remote Control	R. C. Goertz

Report Coordinated by
R. M. Adams and A. Glassner

Issued August 24, 1965

Operated by The University of Chicago
under
Contract W-31-109-eng-38
with the
U. S. Atomic Energy Commission

FOREWORD

The Reactor Development Program Progress Report, issued monthly, is intended to be a means of reporting those items of significant technical progress which have occurred in both the specific reactor projects and the general engineering research and development programs. The report is organized in a way which, it is hoped, gives the clearest, most logical overall view of progress. The budget classification is followed only in broad outline, and no attempt is made to report separately on each sub-activity number. Further, since the intent is to report only items of significant progress, not all activities are reported each month. In order to issue this report as soon as possible after the end of the month editorial work must necessarily be limited. Also, since this is an informal progress report, the results and data presented should be understood to be preliminary and subject to change unless otherwise stated.

The issuance of these reports is not intended to constitute publication in any sense of the word. Final results either will be submitted for publication in regular professional journals or will be published in the form of ANL topical reports.

The last six reports issued in this series are:

January 1965	ANL-7003
February 1965	ANL-7017
March 1965	ANL-7028
April 1965	ANL-7045
May 1965	ANL-7046
June 1965	ANL-7071

Reactor Development Program
Highlights of Project Activities for July 1965

EBR-II

Preliminary examination of the fuel removed after 1.0% burnup indicated an anomalous swelling behavior of the special surveillance samples, although the regular production fuel appeared to be behaving as expected. The special samples were removed from the core for temporary storage in the storage basket, and on July 21 the reactor was started up for operation to the next 0.1% burnup increment.

FARET

The A-E Title II design is essentially complete. All design packages are complete and issued for Packages V and IX. These drawings and specifications have been ready for signature since early June 1965, but approval action is being withheld until the AEC's review of FARET is completed.

ZPPR

The Title II design of ZPPR has been completed somewhat ahead of schedule. Drawings and specifications have been sent to AEC to expedite solicitation of bids. The matrix tubes and nuclear instrumentation (supplied by the Laboratory) have been ordered.

AARR

The Title I indoctrination meetings with the A-E (Burns and Roe, Inc.) are continuing. This indoctrination period is expected to continue through August.

Based on a preliminary stress analysis of the reactor vessel, a design change is being contemplated in which the lower section would be enlarged to eliminate an area of high stress.

TABLE OF CONTENTS

TABLE OF CONTENTS

TABLE OF CONTENTS

I. LIQUID-METAL-COOLED REACTORS

A. EBR-II

1. Operations

The plant was maintained in standby condition until July 21 while awaiting results of fuel inspection at the 1% maximum burnup level. On this date, operation at powers up to 10 MW was accomplished during an 18-hr period for the purpose of making physics measurements prior to the next increment of power operation.

Ten subassemblies containing special surveillance fuel pins were replaced as the result of inspection that revealed they were undergoing swelling at a rate greater than the normal pins and would perhaps be limited to 1% burnup (see Section A.3 below). The special pins in these subassemblies had been precision-measured for dimension and density before they were clad, as part of the fuel-surveillance program. Standard elements in the reactor subjected to varying amounts of burnup up to 1% do not show the same growth, and the reason for the different behavior of the special pins is being investigated. To reduce further the probability of fuel-element failure during reactor operation in the next power run, three subassemblies in Row 3 which had achieved maximum burnup in excess of 0.9% were also replaced with fresh subassemblies.

The reactor was started up on July 29 to begin operation to achieve 1.1% fuel burnup.

2. Systems and Components

a. Rotating Plug-seal Troughs. During preparations for unrestricted fuel handling late in June and during July, it has been difficult to obtain indication of satisfactory temperature distributions in the seal troughs. Furthermore, difficulty was experienced in attempting to initiate the rotation of plugs by motor drive. It was necessary to assist the drive manually in order to loosen the large plug and obtain free rotation.

Because of these difficulties, many samples of the seal-trough tin-bismuth alloy have been taken and chemically analyzed. Of most significance to date is the finding of substantial quantities of metallic oxides in the outer annuli of the troughs. These are accessible for observation and sampling only through the "window holes," one each in the large and small plug dip rings. The "window hole" is a heater hole having a slot approximately 3/4 in. wide extending from the elevation of the trough top to about 3 in. below the alloy surface. Probing with a wire through the window hole of each dip ring has revealed the presence of spongy or crusty layers or deposits in the outer trough annuli, mostly submerged 1 or 2 in. below the molten alloy surface. At month's end, information relative to the distribution of the

deposits around the annuli was not yet available. However, some areas of the trough seem to contain much more material than others.

Samples of these deposits were taken in a syringe device of 3/8-in.-OD tubing containing a plunger. They contain molten metal, black powdery oxide, and porous black clinkers or nodules. Chemical analysis of the oxide portions, especially nodules, of some samples reveals that they are predominantly oxides of bismuth, tin, and sodium. Sodium, as sodium oxide, accounted for 12.5 w/o of one sample. Two other samples showed sodium content corresponding to around 10 w/o of sodium oxide, and the remaining two oxide samples of the five analyzed contained sodium equivalent to 3 or 4 w/o oxide. The iron content of the oxide was very low (less than 1/4 of 1%).

The presence of oxide deposits (or metal-oxide mixtures) in the annuli can plausibly account for plug sticking and also for apparent poor temperature distribution in the troughs. As for the latter, it appears that the oxides blanket some of the upper-level thermocouples, causing low indicated temperatures by interfering with heat transfer from the alloy to the thermocouple. This has been substantiated by probing through the window hole at locations where the thermocouple readings appear too low and thereby obtaining increased temperature readings, apparently by disturbing the oxide deposit and bringing molten alloy into contact with the thermocouples.

Analyses of many metal samples from the troughs have provided no evidence of gross segregation of tin and bismuth. However, sodium content of these samples ranges between 1500 and about 2000 ppm (as Na). It is possible that sodium aerosol or vapor in the primary argon dissolves in the alloy, diffuses through the body of the alloy, and reacts with oxygen in the nitrogen purge gas at the surface of the alloy in the outer annulus. The apparent submergence of the oxide deposits may result from a "plowing" action of the dip ring and adherent deposits during rotation.

Attempts are being made to remove substantial amounts of oxide from the outer trough annuli during molten operation for more detailed examination and to determine whether heat distribution and plug rotation can be improved.

b. Primary Sodium Pump M-1. On July 7, in preparation for a routine check of the pump-control systems, pump No. 1 did not rotate. Prior operating data revealed no abnormality. Total operating time amounted to 4442 hr as of July 7.

A short time before, water had been observed in the vent line from the shield plug of pump No. 1. However, there is no apparent connection between the two occurrences, since the shield plug is totally enclosed and isolated from the sodium tank. Gas analyses of the primary argon showed no increase in hydrogen content as would be expected if water leaked into the primary tank via the pump shaft.

On July 8, the pump shaft-impeller assembly was freed by removing the adjusting nut from the draw stud and tapping until the pump shaft dropped freely. The shaft was then raised by turning the nut on the draw stud. About 150-200 ft-lb of torque was required to start the shaft turning. After rotation had been achieved, the "break-away" torque fell to its original value of about 5 ft-lb. Thereafter, the pump operated normally at rates up to 95% of full flow.

Again, on July 17, the pump could not be started electrically. It was easily freed by lowering and raising the shaft as before. Subsequent startup and operation at rates to 100% were normal.

It is speculated at this time that sticking of the pump shaft may be caused by condensed sodium (along the upper portion of the shaft) which can be sheared by vertical movement of the shaft.

An attempt to dry the shield plug of pump No. 1 by evacuation produced approximately 5 gal of water. The water apparently came from the concrete in the plug.

An attempt was also made to remove any water which might be in the shield plug of pump No. 2 by the same method. However, only a small amount (about 200 ml) was recovered. It appears that the concrete fills the M-2 plug almost completely whereas there is a substantial space in the top of the M-1 plug.

c. Control Rod Drive No. 9. During control rod delatching preparatory to rotating the plugs on July 14, the sensing rod of control drive No. 9 failed to drop under its own weight. It was subsequently freed sufficiently to permit manual movement; however, special attention has been required during fuel handling since then. A spare control rod drive is being readied for replacement when the plant schedule permits.

d. Containment Testing. The rubber seat ring was replaced in a suspect exhaust isolation valve, and the valve was leak-tested satisfactorily. The leak rate of this valve, as measured during its scheduled annual test in May, had been excessive even though the calculated total reactor building leak rate was well under the permissible value.

The annual leak-rate test of the emergency airlock was completed satisfactorily.

e. Sodium and Argon Systems. The plugging temperature of the primary sodium remained below 250°F. The plugging temperature of the secondary sodium was kept below 300°F by intermittent operation of the cold trap.

The composition of the secondary argon remained around 10 ppm hydrogen and 1800 ppm nitrogen.

The primary cover-gas system was purged during the month. After purging, the argon contained less than 10 ppm hydrogen and about 100 ppm nitrogen. Since that time, the hydrogen content has remained below 10 ppm, but the nitrogen content has slowly risen to 1.2 v/o.

3. Fuel Handling

During the period from July 6 through July 16, nine subassemblies were transferred to the Fuel Cycle Facility for disassembly and inspection; they had been removed from the reactor and transferred to the storage basket late in June. These comprised two core-type subassemblies, one core-type inner blanket subassembly, one control rod, one safety rod, two inner blanket, and two outer blanket subassemblies.

After the foregoing transfers had been completed, three experimental irradiation subassemblies were loaded into Row 7 of the reactor. They contain five encapsulated fuel elements of mixed plutonium-uranium oxides supplied by General Electric Company for long-term irradiation at relatively low heat-generation rates as part of the FCR fuel-irradiation program. One of the subassemblies contains one capsule; the other two contain two capsules apiece.

Inspection of the special elements indicated that the limiting burnup for these fuel pins may be only slightly over 1%. Therefore, during the period from July 23 through July 28 the remaining ten subassemblies containing special fuel elements of varying burnup were replaced, as well as three subassemblies from Row 3 of the reactor, each of which had accumulated burnup in excess of 0.9%. One of the latter was replaced by an α-measurement subassembly. In conjunction with the foregoing transfers, six natural uranium core-type subassemblies were removed from the storage basket to reduce the basket inventory. One inner-blanket core-type subassembly was removed to compensate for the increased reactivity of the fresh fuel in the reactor.

4. Reactor Physics

Analysis of zero-power rod drop experiments has established a reactivity worth of the stainless steel rod as 4.08×10^{-4} $\Delta k/k$. Analysis of the 45-MW and 25-MW data, shown in Table V, indicated that the prompt-feedback component is essentially constant between 25 and 45 MW when weighted by the power.

Table V. Zero-power Rod-drop Experiment

Power (MW)	Feedback Reactivity ($\Delta k/k \times 10^4$) Time after Scram (sec) 0.4	0.6
45	0.026	0.047
25	0.015	0.028

5. Fuel Cycle Facility

a. Argon Cell. A radioactively hot bearing was observed on the south fan of the Argon Cell gas-circulation system after about 6000 hr of operation. The contaminated fan and motor were removed and partially decontaminated, and the bearings were replaced. The principal contaminants found were Ce and Zr-Nb, suggesting that dumping of uranium and fission product oxides from the melt-refining crucibles following oxidation is a major source of contamination of the cell atmosphere.

Tests have been made to determine if lubrication can be improved and service life of the fan extended by substitution of a different grease. The fan and motor are being readied for reinstallation.

b. Irradiated Fuel Processing. In a one-month period, six fuel-bearing assemblies and four radial blanket assemblies were freed of sodium and completely dismantled. Six additional unirradiated natural uranium assemblies were also treated to remove sodium. Fuel examination, decanning, melt refining, and oxidation were carried out routinely.

c. Fuel Surveillance. The core-type subassemblies removed for inspection contained fuel pins which had been selected for special pre- and post-irradiation examination by Metallurgy Division as part of the fuel-surveillance program. In the original program to survey the fuel in EBR-II for the effect of incremental increase in burnup, a series of 15 core subassemblies (91 element) was made up which included seven specially prepared and centrally located elements. This special preparation included dimensional and density measurements with greater accuracy than the normal production measurements.

Five surveillance subassemblies, representing maximum burnups of 1.0, 0.9, 0.8, 0.7, and 0.5%, have been partially examined. Although the examinations are not yet complete, probably the most significant measurements (sodium level as an indicator of volume change) have been made on these subassemblies. In addition, subassembly C-145 (maximum burnup of 0.935%) has also been subjected to sodium-level analysis. This sixth subassembly was added to the initial program to confirm data and conclusions derived from the first five.

A comparison of the postirradiation measurements of sodium level of the seven special elements of a subassembly and a sample of the normal elements surrounding these indicates the average level of the seven is higher than the average level for the normal production elements. This has led to the removal from the reactor of those subassemblies containing the special elements.

The data for the sodium level of elements from the six surveillance subassemblies are shown in Table I.

Table I

Subassembly No.	Position	Calculated Max Burnup[b]	Average Sodium Level (in. above Fuel Tip)	Number of Elements Measured
C-138	1A1	1.00	1.30	21
C-138 K[a]	1A1	1.00	1.65	7
C-145	2E1	0.935	1.33	81
C-145 K[a]	2E1	0.935	1.56	7
S-601	3D1	0.881	1.30	21
C-141	4C1	0.804	1.12	21
C-141 K[a]	4C1	0.804	1.21	7
L-410	5E3	0.687	1.12	21
B-314	6E4	0.500	1.02	21

[a]K designation refers to the special elements.
[b]Burnup expressed as atom percent of heavy atoms.

Earlier data obtained from subassemblies which included the special elements are shown in Table II.

Table II

Subassembly No.	Position	Calculated Max Burnup[c]	Average Sodium Level (in. above Fuel Tip)	Number of Elements Measured
C-140	2A1	0.261	0.70[b]	21
C-140 K[a]	2A1	0.261	not measured	-
C-143	2C1	0.498	0.91	21
C-143 K[a]	2C1	0.498	1.01	7

[a]K designation refers to the special elements.
[b]Average sodium level as manufactured is 0.688 in.
[c]Burnup expressed as atom percent of heavy atoms.

The data of Tables I and II clearly indicate a larger volume increase (as indicated by sodium level) in the special elements than in the normal production elements. The sodium-level data shown in Table I are for core elements (C), safety rod (S), control rod (L), and a sixth row core (B). Previous data accumulated for core elements show a fairly regular increase in sodium level with increase in burnup. Although not conclusively

defined, there is initial evidence that the sodium levels of safety and control subassemblies are somewhat higher than those of comparable core subassemblies. The sodium level numbers for control and safety elements may be biased because of a possibly higher void content caused by the acceleration in operation.

Pressure-volume measurements of 10 elements from each of two of the subassemblies (C-138 and C-141) are shown in Table III.

Table III. Pressure-volume Data

Subassembly No.	Calculated Max Burnup[a]	Average Void Volume (cc)	Average Pressure (psia)
C-138	1.00	0.304	21.8
C-141	0.804	0.354	18.6
Unirradiated	0.0	0.487	14.7

[a]Burnup expressed as atom percent of heavy atoms.

Dimensional comparison before and after irradiation of the normal production pins from subassembly C-138 has been completed. A significant (to this study) increase (up to 0.004 in.) in the maximum and minimum diameters was noted. These data are shown in Table IV. Three of the pins showed length increase, while the remaining pins were shorter than when manufactured.

Table IV. Diameters of Pins from Subassembly C-138

	Minimum Diameter (in.)		Maximum Diameter (in.)	
Pin No.	Before	After	Before	After
5	0.1418	0.1435	0.1450	0.1459
12	0.1423	0.1435	0.1441	0.1465
19	0.1428	0.1435	0.1442	0.1481
27	0.1427	0.1443	0.1439	0.1471
65	0.1426	0.1445	0.1444	0.1472
73	0.1425	0.1450	0.1437	0.1478
80	0.1426	0.1445	0.1450	0.1471
86	0.1424	0.1445	0.1443	0.1463
58	0.1422	0.1450	0.1443	0.1474

B. FARET

1. General

The FARET architect-engineering (AE) portion of the Title II Design is essentially complete. All design packages are complete and issued except Packages V (Instrumentation and Control) and IX (General Facility).

Design Packages V and IX drawings and specifications have been ready for signature since early June 1965, but approval action is being withheld until the AEC's review of the FARET project is complete.

The current delay in authorizing the initiation of Title III continues to multiply problems of schedule and cost estimates. The liquid-metal heat-exchanger procurement, Package III, and the liquid-metal pumps procurement, Package IV, are becoming dominating factors in establishing the construction schedule. In addition, costs continue to increase as a consequence of changing market conditions.

2. Port Seal of Fuel and Equipment Transfer System

The fuel and equipment transfer system (see Progress Report for December 1964, ANL-6997, p. 21) incorporates a port seal (see Figure 1) which must be engaged between the transfer port and the fuel cask during fuel-transfer operations.

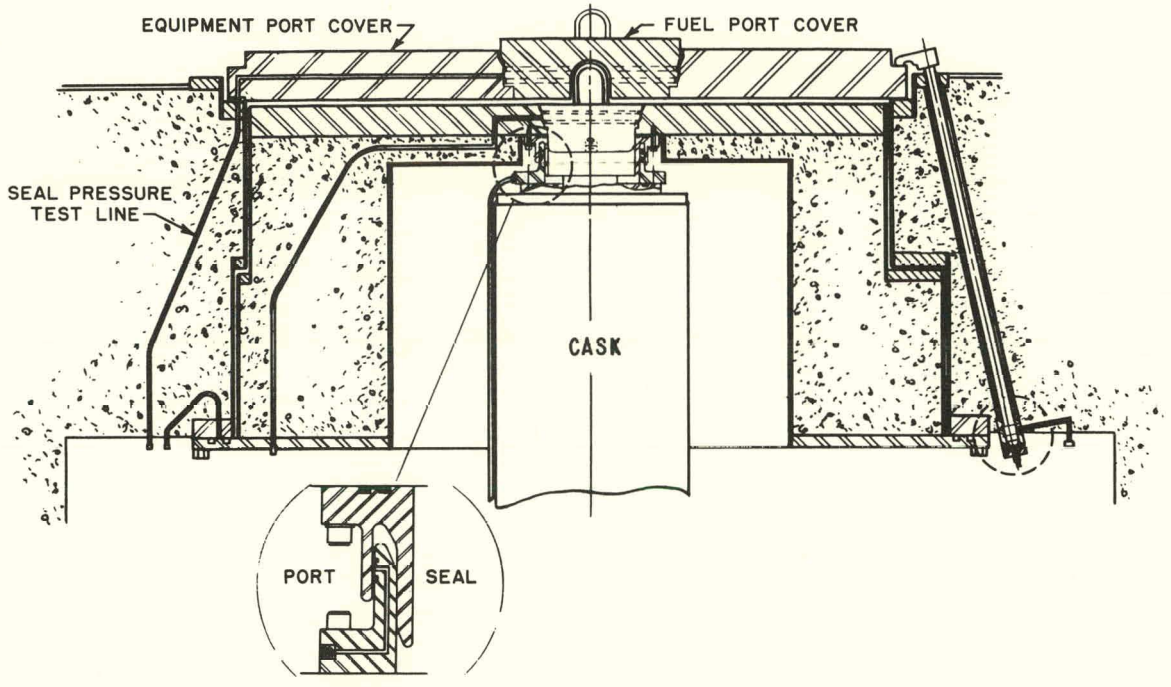

Figure 1. Fuel and Equipment Transfer Ports

A test fixture (see Figure 2) has been designed for the testing of a full-scale mock-up seal to determine the operational performance and leak rate up to 30 psi of the seal. In this fixture it will be possible to simulate the loading and positioning of the fuel cask at the maximum allowable specified misalignment of 1/2 in.

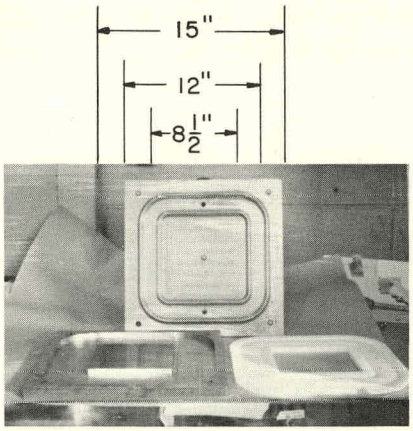

Figure 2
Vault Seal Leak Rate Test

Since the port seal will be subjected to frequent service and wear, highly wear- and load-resistant materials have been selected for the test as follows.

a. The guide-seal materials are Adiprene 'O' rings for relatively high gamma-radiation (5×10^9 R) resistance with the surface Teflon impregnated to provide a low coefficient of friction (0.04) during seal mating (the adequacy of the seal should not be affected by the lower radiation-damage threshold of the Teflon).

b. AISI-4140 forging material, heat treated to a hardness of $R_C 38$ for the mating parts, to obtain excellent wear- and load-resistant properties.

c. Chromium plating on the mating surfaces to obtain a low coefficient of friction (~0.01).

It is also planned to impose lateral loadings by means of a hydraulic cylinder to simulate specified seismic conditions of approximately 700 lb.

3. Fuel Assembly Sodium Flow Test Loop

All welding of the sodium pipe lines is completed and has passed radiographic inspection. The upper spool piece has been placed in position. The installation of the thermal insulation continues.

Welding of the 2-in. drain lines from the loop to the dump tank has been completed, and steps are now underway to helium leak check the entire FARET loop piping prior to sodium filling.

Sodium flow has been established in the plugging-meter circuit of the old vertical sodium dump-tank auxiliary cleanup loop. Several plugging runs have been made and one static sample has been sent for oxygen analysis. Results of plugging-meter determinations (5 separate runs) of oxide content confirm the chemical analysis report of 19 ppm oxygen. For example, plugging temperatures are from 210°F to 230°F, which are very low.

4. Static Test Facility

Satisfactory fabrication drawings of the 66-in.-diameter pressure vessel (see Progress Report for April 1965, ANL-7045, pp. 10-11) and a stress analysis of the weld neck flange have been received from Stearn-Rogers Mfg. Co., the vendor. The construction bids for the pit in Building 206 were excessive; action was taken to relocate the pit to effect a sizable cost reduction.

5. Control-rod Drives

a. Control-rod-drive Shock-absorber Test. A shock-absorber test facility (see Figure 3) was assembled in the test laboratory during the months of June and July. The shock absorber utilizes a stepped piston and a straight annular cylinder filled with oil to absorb the energy of the moving parts of the control drive and the control rod at the end of the downstroke during scram conditions. The dimensions of the shock-absorber plunger and annular cylinder were established by equating the energy of the accelerated mass (1.5 g) and the energy of the oil flowing past the annulus formed by the stepped piston and cylinder.

Preliminary test results showed good agreement with the calculations, i.e., there was no noticeable shock or impact between the piston and the bottom of the cylinder. A plot of rod displacement versus time (see Figure 4) showed satisfactory acceleration and deceleration characteristics.

b. Test Facility for Control-rod Electrical Components. The facility (see Figure 5) to test electrical components under load conditions in a 150-160°F argon environment for a lengthy period of time is being assembled in the test laboratory.

The facility consists of a sealed argon tank which is large enough to contain gear-motor units and various types of limit switches. A cal-rod heater, thermocouples, and a temperature controller are used to maintain the argon temperature between 150 and 160°F. The proposed FARET control-drive gear motor is installed within the tank with the output shaft penetrating through a suitable shaft seal. Outside the tank, connected to the output shaft, is a series of gears and a sprocket with the load tray to simulate the control-drive load and speed on the gear motor. A second output shaft within the tank drives a screw to which is attached several switch-actuating cams for operation of the switches under test.

c. Test of Bellows Seal. The control-rod drive-shaft bellows seal has successfully accumulated 7,567 cycles (for previous test results see Progress Report for May 1965, ANL-7046, p. 6).

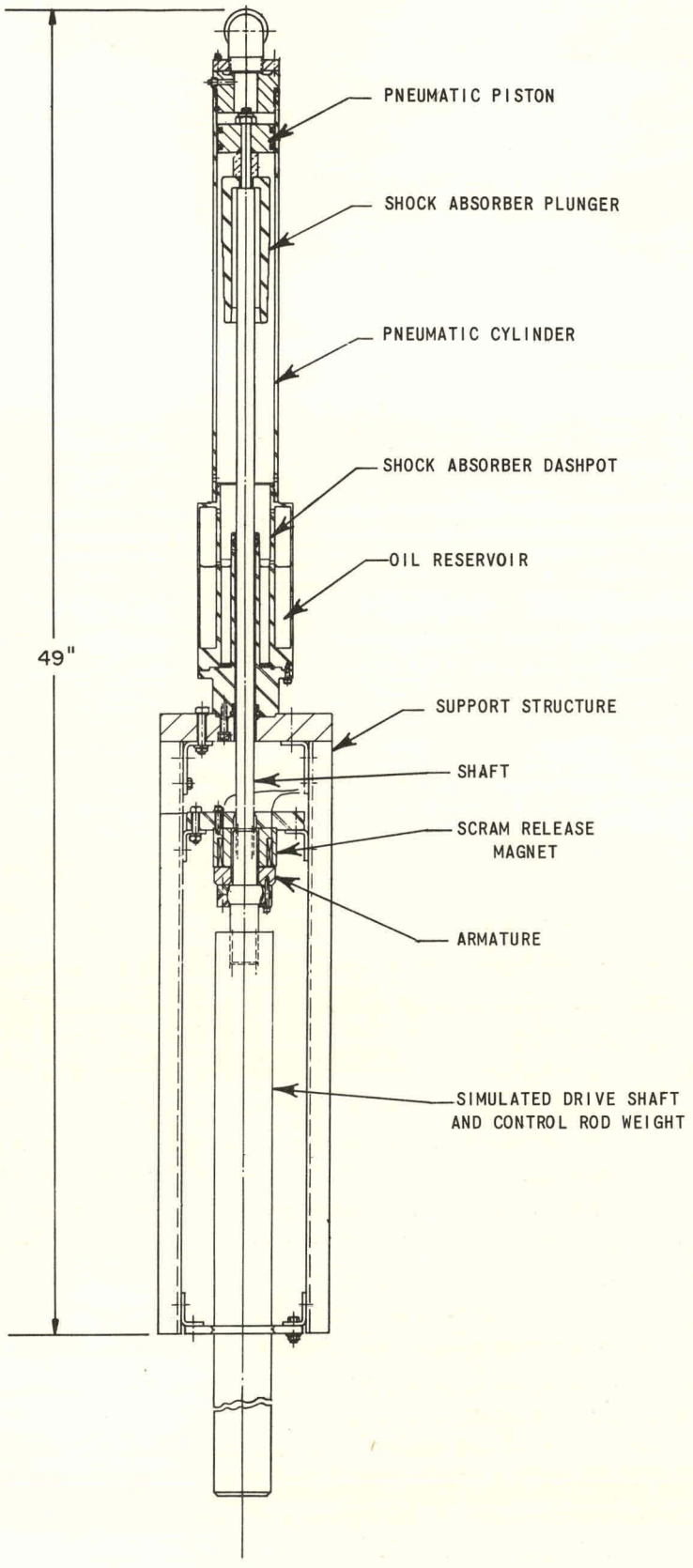

Figure 3. Shock Absorber Test Facility

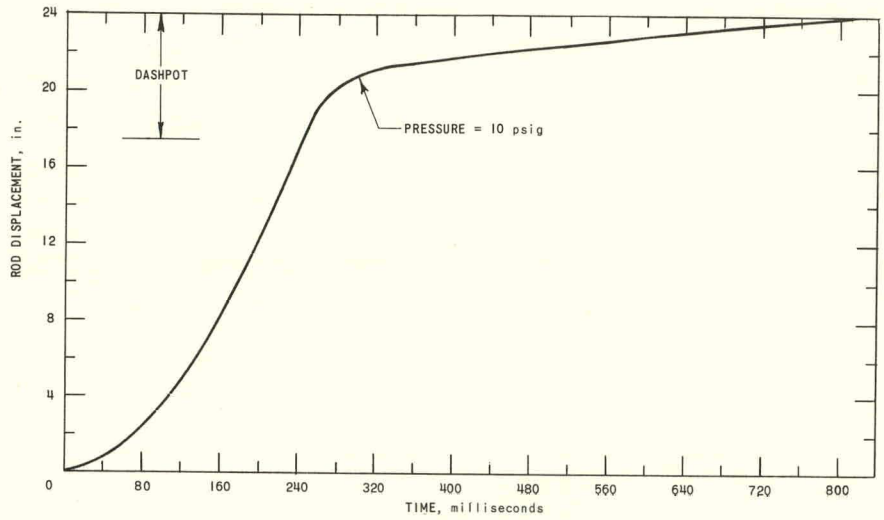

Figure 4. Displacement vs. Time

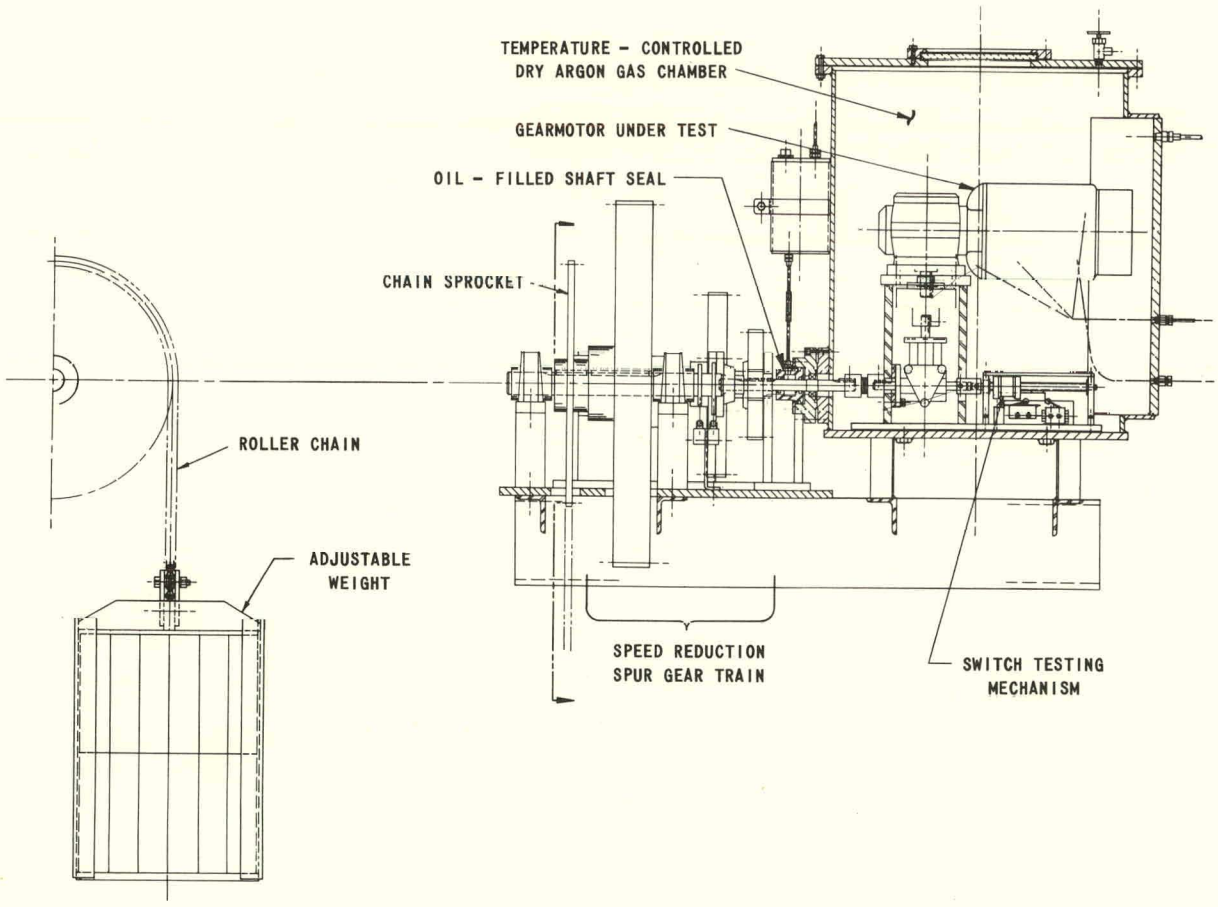

Figure 5. FARET Control Rod Drive Mechanism--Electrical Equipment Test Apparatus

6. Vault Hatch Seals

The vault is an extension of the cell-containment structure and is used to house the equipment and systems directly related to the operation of the reactor and some cell components. For this reason criteria for vault containment are the same as for the cell. Access to the vault is primarily through hatches which are used occasionally for equipment installation and removal. These hatches are bolted and sealed when the reactor is in operation. In order to provide for testing without pressurizing the entire containment, a double seal was designed (see Figure 6).

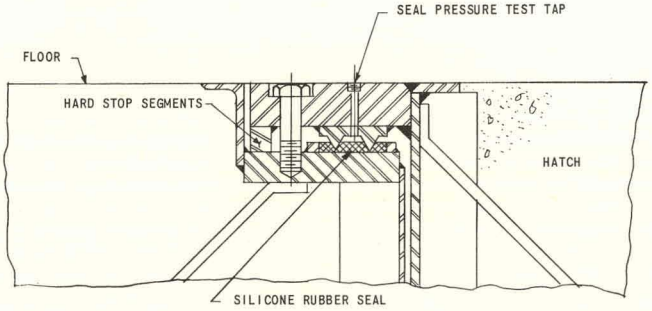

Figure 6

Vault Hatch Seal

A test was designed to measure leak rates at 30 psi at various compression of the seal to ascertain the adequacy of the seal design. The test fixture (see Figure 7) is comprised of 40 in. of seal and four corners. The test results to date using air are summarized in Table VI. The test leak rates are many orders of magnitude ($\sim 10^6$) below the allowable design leak rates.

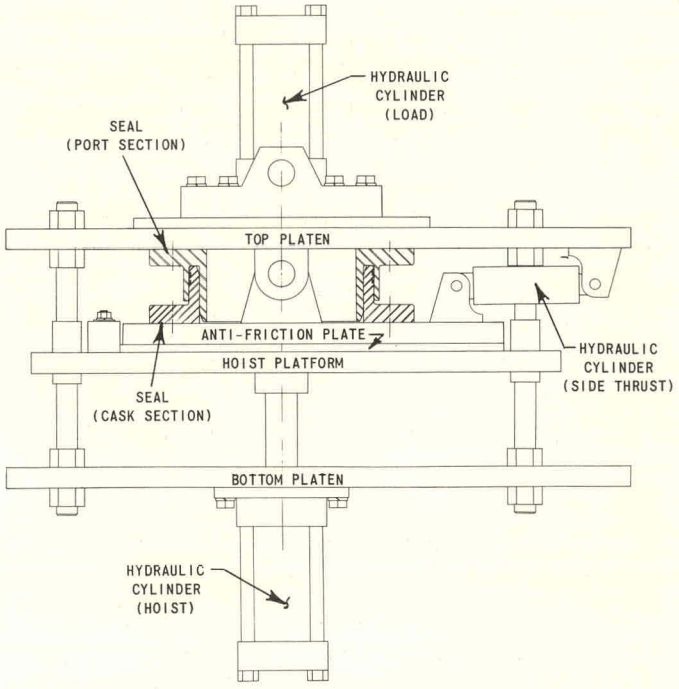

Figure 7. FARET Fuel and Equipment Transfer System Guide-Seal Test Fixture

Table VI. Results of Leak-rate Test of Vault Hatch Seal

(air at 30 psig)

Seal Compression, in.	Leak Rate of Test Fixture	Leak Rate per Linear Foot of Seal
1/8	8.25×10^{-3} cu ft/day 3.15×10^{-8} lb/day	2.5×10^{-3} cu ft/day 9.5×10^{-9} lb/day
1/4	3.9×10^{-3} cu ft/day 1.5×10^{-8} lb/day	1.2×10^{-3} cu ft/day 4.5×10^{-9} lb/day
3/8	1.5×10^{-3} cu ft/day 6.0×10^{-9} lb/day	4.5×10^{-4} cu ft/day 1.8×10^{-9} lb/day

Tests are under way to determine if the seal can be reused and to determine the effect of distortion on the leakage rate. Tests using argon gas will be made in several cases to confirm the calculated leak rates based on the use of air.

Additional tests will determine whether or not the sealing material must be replaced after each hatch opening.

7. FARET Criticals

Experiments with Core F of Assembly 46 of ZPR-3, a mock-up of a possible multifuel-zoned core loading for FARET, were done. The FARET core design simulated consists of a central zone of 7 oxide-fueled (PuO_2-UO_2) subassemblies, a third subassembly ring of 12 carbide-fueled (PuC-UC) elements, the fourth ring, with 18 subassemblies, containing the oxide fuel, and the fifth ring composed of 12 more oxide subassemblies alternating with 12 subassemblies of a Zr-Pu-U alloy metal fuel. Core 46D (see Progress Report for June 1965, ANL-7071, p. 16), an earlier mock-up design of this multizone system was found to be too reactive. A subsequent design, called 46E, was started in early July, but was discontinued when the indicated critical volume was found to be too large to represent the 61-subassembly FARET system. A readjustment of the zone fuel enrichments provided the Core F design and the desired mock-up geometry. Experiments completed with the 46F core include fuel interchanges in the different core zones and measurements of reactivity worth of mock-up FARET B_4C control rods.

In Core D, the average uranium enrichments of the three fuel-type simulations were 40% for the oxide, 49% for the carbide, and 12% for the alloy. The compositions closely approximated those specified for a postulated initial loading of the FARET core. The mock-up design, however, provided a critical core loading equivalent to about 51 FARET subassemblies, compared to a designed 61-subassembly representation. Consequently, the U^{235} enrichments in all three of the fuel simulations were reduced to 33% in

the oxide, 37% in the carbide, and 6% in the alloy, in the core designated 46E (see Table VII).

Table VII. Core Zone Compositions for ZPR-3 Assembly 46E

Loadings of 0.7807-liter core sections (25.48 x 5.54 x 5.54 cm) of oxide, carbide, and alloy fuel simulation drawers.

	Composition, g/cc			Composition, 10^{22} atoms/cc		
Material	Oxide	Carbide	Alloy	Oxide	Carbide	Alloy
$Pu^{239 + 241}$	0.424	0.621	1.045	0.107	0.156	0.263
$Pu^{240 + 242}$	0.020	0.030	0.050	0.005	0.008	0.013
U^{235}	0.876	1.307	0.218	0.224	0.335	0.055
U^{238}	1.810	2.217	3.575	0.459	0.561	0.904
$U^{234 + 236}$	0.013	0.019	0.003	0.003	0.005	0.001
Na	0.321	0.321	0.321	0.843	0.843	0.843
O	0.230	-	-	0.866	-	-
C	0.100	0.220	-	0.502	1.111	-
Fe	1.019	0.981	1.058	1.099	1.057	1.141
Cr	0.255	0.246	0.265	0.295	0.284	0.307
Ni	0.141	0.136	0.147	0.145	0.140	0.144
Zr	-	-	0.480	-	-	0.317

The approach to critical with Core 46E was terminated at a subcritical loading of 124 drawers (equal to about 62 subassemblies); the approach curves extrapolated to a critical loading of about 138 drawers (69 subassemblies). Indications were that the critical loading would contain 12 oxide and 12 alloy core drawers of the fifth ring, and probably 3 oxide and 4 alloy units in the sixth ring of core drawers in each assembly half. To reduce the critical volume and eliminate loading in a sixth ring, it was decided to increase the uranium enrichments in the carbide and alloy fuel simulations, and a new approach-to-critical was begun with core 46F.

For the Core 46F design, the uranium enrichment in the alloy fuel drawers was returned to 12%, that in the carbide was raised to 45%, and in the oxide the enrichment was left at 33%. Table VIII gives the compositions of these three fuel simulations in Core 46F, and Figure 8 illustrates the hexagonal core arrangement mocking up the FARET geometry. Except for the 51-cm core length for Core 46F, the dimensions and compositions of the various reflector regions shown are the same as specified for Core 46B. The 61 core drawers per assembly half loading shown in Figure 8 had an available excess reactivity of 100 Ih at an average core temperature of 38°C.

The zoned-core loading of a system like FARET introduces the hazard of inserting a particular fuel-type subassembly in the wrong fuel zone. An evaluation of the associated reactivity effects for such

occurrences was made in a series of fuel-interchange experiments in Half No. 1 of the assembly. Core drawers with 0.78-liter core sections of a fuel type (oxide, carbide, or alloy) were substituted for drawers of the other fuel types in their respective zones, with emphasis on replacements of alloy and carbide core drawers for the less reactive oxide fuel drawers. Replacements of reflector with fuel in the sixth ring were also done. Table IX lists the core locations of the experiments and the results of the substitutions.

Table VIII. Core Zone Compositions for ZPR-3 Assembly 46F

Loadings of 0.7807-liter core sections (25.48 x 5.54 x 5.54 cm) of oxide, carbide, and alloy fuel simulation drawers.

	Composition, g/cc			Composition, 10^{22} atoms/cc		
Material	Oxide	Carbide	Alloy	Oxide	Carbide	Alloy
$Pu^{239 + 241}$	0.424	0.621	1.045	0.107	0.156	0.263
$Pu^{240 + 242}$	0.020	0.030	0.050	0.005	0.008	0.013
U^{235}	0.876	1.600	0.437	0.224	0.410	0.112
U^{238}	1.815	1.866	3.351	0.459	0.472	0.848
$U^{234 + 236}$	0.013	0.019	0.006	0.003	0.005	0.002
Na	0.321	0.321	0.321	0.843	0.843	0.843
O	0.230	-	-	0.866	-	-
C	0.100	0.220	-	0.502	1.111	-
Fe	1.019	0.981	1.058	1.099	1.057	1.141
Cr	0.255	0.246	0.265	0.295	0.284	0.307
Ni	0.141	0.136	0.147	0.145	0.140	0.144
Zr	-	-	0.480	-	-	0.317

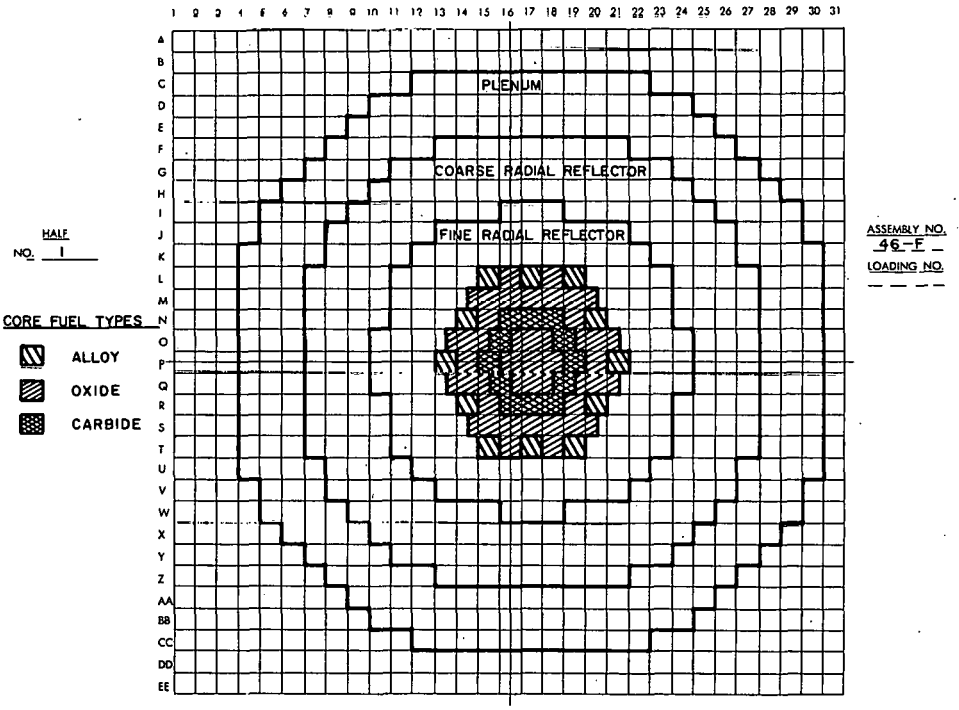

Figure 8. Interface View of ZPR-3 Assembly 46F

Table IX. Fuel Interchange Experiments in ZPR-3 Assembly 46F

Fuel-type compositions as specified in Table VIII; reflector composition, 0.211 g/cc Na, 6.38 g/cc stainless steel, 0.305 g/cc Al.

Drawer Location*	Substitution in 0.78-liter Core Section	Reactivity Change (Ih)
1-P-17	Carbide for oxide	+198
1-P-17	Alloy for oxide	+107
1-Q-17	Carbide for oxide	+191
1-R-17	Alloy for carbide	- 75
1-S-17	Carbide for oxide	+132
1-S-17	Alloy for oxide	+ 70
1-T-17	Oxide for alloy	- 42
1-T-18	Alloy for oxide	+ 41
1-U-17	Oxide for reflector	+ 75
1-U-17	Carbide for reflector	+136
1-S-14	Reflector for oxide	-107

*See Figure 8.

A program of B_4C control rod mock-up studies was carried out to evaluate the basic design of the FARET control-rod system. The reactivity and burnup control of FARET will be provided by 12 enriched B_4C poison rods located around the core. Mock-ups of four of these rods, simulating about 55 v/o B_4C, 19 v/o Na, and 17 v/o steel, were made in ZPR-3, and the reactivity effects of various stages of insertion of the rods were measured subcritically. Preliminary analysis of the results indicates a loss of 1150 Ih (about 2.2% $\Delta k/k$) for moving four 70 a/o enriched rods in 20 in.

Radial traverse experiments were initiated with fission counters and reactivity samples.

C. General Fast Reactor Physics

1. Doppler Measurements with ZPR-6

Doppler measurements are being made with Assembly 4Z (see Progress Report for May 1965, ANL-7046, p. 14) using a heated-sample technique. The work with U^{238} and with the reactor composition samples (7/1 U^{238}/U^{235}) has been completed, and a start has been made on the samples containing higher fractions of U^{235}.

The effect of thermal expansion of a sample in the axial direction on the measured reactivity effect has been measured for both U^{238} and 7/1 $\sigma^{238}/\sigma^{235}$ samples by comparing measurements for two samples identical except that free expansion was allowed in one case and axial expansion

was not allowed in the other. (Special elements were designed to make this possible.) A small negative reactivity effect due to expansion was observed for the 7/1 samples; the U^{238} samples gave a small positive effect. Both are consistent with calculated estimates of the expansion effect in sign and in magnitude.

The measurements on the effect of variation of rod size with 1-in., 3/4-in., and 1/2-in.-dia UO_2 samples on the Doppler effect were completed. The measured effect increased with decreasing rod size. The difference in reactivity per unit mass of sample was about 20% between the 1/2-in. and 1-in. samples; the 3/4-in. sample gave results much closer to those of the 1/2-in. rather than the 1-in. sample.

The effect of carbide versus oxide fuel samples was tested with a 1/2-in.-dia U^{238} carbide sample. A direct comparison of the 1/2-in. oxide and carbide results is not possible because the carbide is considerably more dense, but the carbide result did fall about midway between results found for 1/2-in. and 1-in. oxide samples.

Finally, a test was made to demonstrate that the measured effects are, in fact, due to low-energy neutrons. A 1/2-in.-thick boron carbide filter was installed around the 1-in. UO_2 sample. This sharply reduced the number of neutrons in the Doppler energy region but did not, according to calculation, remove all the neutrons in the upper Doppler energy region. The measured reactivity effect was about 20% of that without the boron filter, in agreement with the calculation.

2. On-line, Computer-processed, Central-rod Calibration in ZPR-9

The DDP-24 computer has been set up in conjunction with ZPR-9 to provide routine on-line processing of rod-calibration data in an arrangement that is an extension of the off-line processing method (see Progress Report for January 1965, ANL-7003, p. 9). Starting with the reactor critical, the rod is slowly moved in the direction of decreasing reactivity. Flux information is taken from the input data scalers and converted to reactivity as received.

Rod motion is monitored by counting pulses produced by a microswitch actuated by a cam on the rod-position-indicator shaft. Special circuitry is provided to eliminate the effect of contact bounce and to prevent a pulse from being missed if it occurs while the scalers are feeding information into the computer.

Flux information is obtained from a voltage-to-frequency concerter connected to one of the current amplifiers which is part of the reactor-instrumentation system. This gives much better statistics than a pulse

counter, since a moderate ion chamber current represents far more events per second than a pulse counter can handle. Consequently, previously noted fluctuations in the reactivity curves have been greatly reduced.

The beginning and end of a run are marked by the reactor operator with a switch connected to one of the computer sense lines, just as for the on-line period measurements. After a run is complete, the integral worth curve for the rod is drawn by the computer graph plotter. A suitable scale is chosen so that the curve fills the graph, which is annotated with the appropriate scale markings.

The system has been in routine use for rod calibrations for ZPR-9. It has been used for rods worth up to 160 Ih, and its results have agreed accurately with calibration curves obtained from positive period measurements.

3. ZPPR

The detailed design of the ZPPR facility (Title II) was completed. The Title II drawings and specifications were transmitted to the AEC to expedite early solicitation for bids.

Review of the Preliminary Safety Analysis Report was held with the subcommittee of the ACRS on July 7. As a result of their recommendation, preparations are now being made for coring of the gravel of the Gravel Gertie test structure and analysis of the coring.

The outside electrical and steam-systems package is approximately 55% complete, and on schedule toward the completion date of August 24.

The steel beam posts for the pilings of the ZPPR structure were received July 23. Five of the 53 posts appear to have been slightly damaged upon arrival. The vendor has been contacted for disposition.

The following is a status report on reactor components:

a. Reactor Bed and Tables. Preliminary machine design drawings by the vendor, Giddings and Lewis Machine Co., Fond du Lac, Wisconsin, are essentially completed.

b. Matrix Drawers. The design work on the form tooling has been completed by the vendor, Mechanical Products Mfg. Co., Seattle, Washington, and shop work is about 30% complete. Design work on the perforating die has also been completed, and shop work has started. The shop work on the test tube assembly has commenced.

c. Matrix Tubes. The order for the matrix tubes was placed on July 21 with Van Vetter, Inc., Seattle, Washington, who proposes to fabricate the tubes from sheet metal. This is a different method of fabrication than has been used for ZPR-3, ZPR-6, and ZPR-9. The method appears feasible; if the supplier is able to produce these by this method within the specification, this may provide a more economic source of these components.

d. Fuel Rod Drives. The fabrication of the fuel-rod drives by McGee-Hogan of Salt Lake City, Utah, is approximately 40% complete. The prototype rod drive has been subjected to approximately 400 complete cycles of operation with no malfunctions. Travel times for rod scrams were measured. Total times, including the magnet relay and manual scram switch, for 90% of travel (21.6 in.) with the rod drive attached to a loaded control drawer inserted into a matrix tube are as follows:

Drawer Loading (lb)	Total Time Lapse (ms)
35	210
26	190
0	165

The drive rod test assembly was dismantled and placed in storage.

e. Poison Safety Rod Drives. The bid package for the poison safety rod drives has been sent to prospective bidders. The bids are due back August 9.

f. Nuclear Instrumentation. Specifications have been completed and reviewed and a service request has been issued for their procurement.

D. General Fast Reactor Fuel Development

1. Metallic Fuels

a. Compatibility of Improved U-Pu-based Fuels with Potential Cladding Materials. The recent finding that Type 304 stainless steel was compatible with U-18.5 w/o Pu-14.1 w/o Zr up to 800°C (see Progress Report for May 1965, ANL-7046, p. 19) has encouraged us to make a systematic investigation of the U-Pu-Zr alloys with 304 stainless steel and other iron- and nickel-base alloys. Some results obtained with 304 stainless steel, Hastelloy-X and Incoloy 800 are given in Table X. The important points to be noted are:

(i) A decreasing zirconium content in the fuel lowers the temperature at which melting of the reaction products occurs for both iron- and nickel-base alloys.

(ii) Type 304 stainless steel shows better compatibility (that is, a higher melting temperature) than either Hastelloy-X or Incoloy 800. This suggests that increasing nickel content in the cladding degrades its compatibility with the fuel.

(iii) The reaction layers formed at temperatures below melting are very thin, suggesting good compatibility for extended periods. Preliminary extrapolation of the short-time data at 650°C to one year predicts about a 4μ reaction layer for the U-Pu-Zr/304 stainless steel combination.

Table X. Fuel Penetration into 304 Stainless Steel, Hastelloy-X, and Incoloy 800 Cladding

		Penetration (cm x 10^4)								
		U-16.6 w/o Pu-6.3 w/o Zr			U-15 w/o Pu-10 w/o Zr			U-18.5 w/o Pu-14.1 w/o Zr		
Cladding	Temp (°C)	7 days	17 days	42 days	7 days	17 days	42 days	7 days	17 days	42 days
304 Stainless Steel	650							<1		
	700		8			2		1	2	6
	750	*Melted			4			2		
	800							9		17
	850							*Melted		
Hastelloy-X	700		50			10				12
	750	*Melted			*Melted					
	800							*Melted		*Melted
Incoloy 800	750				16		38			
	800				*Melted					

*Melting of the reaction products and accelerated penetration occurred.

In an effort to explain the improved compatibility of U-Pu-Zr alloys we simplified the system under study from U-Pu-Zr//304 SS to U-Zr//Fe. Two areas were then investigated:

(i) The compatibility of U-Zr binary alloys with iron to determine if their interaction was similar to the U-Pu-Zr//304 SS interaction;

(ii) Phase relationships in the U-Zr-Fe ternary to determine if the formation of liquid phase in the U-Fe system is suppressed by the addition of zirconium.

Compatibility tests in the U-Zr//Fe system showed that melting of the reaction products is prevented at 800°C in U-Zr alloys containing more than 9.7 w/o Zr, in agreement with results obtained with the U-Pu-Zr//304 SS system. Furthermore, the phase studies indicated that the formation of liquid phases is suppressed up to 800°C in U-Zr-Fe alloys containing zirconium concentrations in excess of 9.7 w/o. These two areas of agreement substantiate the opinion that it is indeed the addition of zirconium to the U-Pu alloys that improves its compatibility with stainless steel rather than a possible side effect.

2. Jacket Materials

a. Vanadium Alloys. Vanadium-titanium-base alloys have generally favorable combinations of properties for use as jacketing materials for various potential fast-reactor fuels, including the uranium-plutonium-fizzium fuel alloys. Since previous tests have shown that vanadium-20 w/o titanium (TV-20) is one of the outstanding vanadium-titanium alloys for uses of this type, the fabrication development of TV-20 jacket tubes is being pushed in all its stages; also, the properties of TV-20, including corrosion behavior in oxygen-bearing sodium and the effects of modifying the composition, are being investigated.

Additional TV-20 tubing has been received from the Superior Tube Company, who drew three tube-blanks furnished by ANL to a final size of 0.653-cm ID x 0.051-cm wall. Of a total of 23.2 m of tubing received, representing a 78% yield (not including pieces of finished tubing shorter than the required 61-cm minimum length), 22.5 m exhibited no defects equal to or greater than 10% of the wall thickness. The 0.7 m of defective tubing contained three small defects, with two being $<10\%$ and one (a lap) being approximately 10% of the wall in depth.

As this is the second batch of high-quality tubing received from Superior Tube Company, it can be concluded that commercial tube-drawing of this alloy has been demonstrated assuming that high-quality tube-blanks are furnished for redraw.

The basic components for a high-velocity pumped sodium loop (i.e., the EM Pump and EM Flowmeter) have been received. The electrical wiring is currently nearing completion, and the shop is constructing the necessary sample sections. Flow velocities of up to 9.1 m/sec should be possible at temperatures up to 650°C. Provisions have been made for a cold-trap bypass and another leg which may be used for the installation of either a "plugging valve" or a hot trap. This test equipment will be used to evaluate the dynamic corrosion behavior of those alloys which have demonstrated resistance to static sodium.

Additional points were determined for the corrosion curve of TV-20 in sodium (containing 50 ppm oxygen) under static conditions. The thickness loss was proportional to the exposure time (0-7 days). The loss rate was approximately 0.8×10^{-3} cm/day on each surface. To this the oxygen penetration into the metal should be added to determine the total metal loss. The latter values have not been obtained as yet for this experiment.

The problem of obtaining representative sodium samples at elevated temperatures for oxygen analysis is still under investigation. Initial results of tests in which nickel and stainless steel sample tubes were used were inconclusive in determining if reduction of oxide formed on stainless

steel at room temperature is the cause of consistently high oxygen values found for zirconium-gettered sodium samples withdrawn at high temperatures.

A new sampling technique is being developed that will permit flushing of the sampling tube with sodium from the liquid metal bath prior to pulling a sample for analysis.

Exposure of TV-20 specimens in zirconium-hot-gettered sodium at 550°C is now in progress.

3. Fuel for Zero-power Reactors

a. Titanium Alloys. The air-corrosion tests of the U-19 a/o Pu-3 a/o Ti and U-25 a/o Pu-5 a/o Ti alloys (see Progress Report for May 1965, ANL-7046, p. 30) have been terminated, as both specimens completely disintegrated. The former required 58 weeks to disintegrate and gained 14.4% in weight; the latter disintegrated in 21 weeks and gained 12.8% in weight. The U-25 a/o Pu-10 a/o Ti alloy is still being tested and, after 21 weeks, has gained no further weight since the original weight gain of 0.3% after 13 weeks. An alloy of U-25 a/o Pu-12 a/o Ti similarly tested has shown no powdering or weight gain after 10 weeks (the U-25 a/o Pu-10 a/o Ti powdered slightly and gained 0.2% in weight after 10 weeks).

b. SEFOR Fuel. The two SEFOR fuel plates (see Progress Report for February 1965, ANL-7017, p. 34) show no swelling or other evidence of fuel instability after storage for 1 year.

Two SEFOR fuel plates manufactured by NUMEC are being tested, one for long-term storage and one for simulated weld failure. On the latter a small notch was filed through the weld on one side of the jacket. No contamination was detected. A much larger notch was filed through the weld on the opposite side and the two faces of the jacket separated slightly in order to expose the fuel. Approximately 10,000 dpm were detected directly over this notch. After 3-mo storage in an air-atmosphere glovebox, the fuel plate has shown no swelling or further spread of contamination.

A similar test of a simulated weld failure has been started on a ZPR-3 fuel plate of Pu-1 w/o Al alloy. Approximately 100,000 dpm were detected directly over a large notch filed in the jacket, but at a distance of one inch from the notch no α activity could be detected.

Both notched fuel plates are being kept in a clean, air-atmosphere glovebox. They will be checked periodically for swelling and for powdering of the fuel. The glovebox will be monitored to see if any spread in contamination occurs.

c. Design and Fabrication Methods. This program aims to develop a commercially applicable design and to investigate potentially low-cost methods for making ZPPR and ZPR-6 fuel elements. Plate castings have been made of the following alloys to provide materials for ignition tests and for determining fabrication characteristics: (i) U-25 w/o Pu-2.5 w/o Mo; (ii) U-25 w/o Pu-2.75 w/o Ti; (iii) U-20 w/o Pu-2.5 w/o Mo. (The latter material is that being used for the ZPR-3 SEFOR critical tests.)

Plates of the U-25 w/o Pu-2.5 w/o Mo were rolled. A single-pass reduction of 30% was made under the following conditions: (i) the billet temperature was 650°C; (ii) roll temperatures were 260°C; (iii) the roll speed was 76.2 m/min; (iv) the roll diameter was 7.7 cm. The resulting strip had rough edges but no lateral cracks. The same amount of reduction was made with the billet at 610°C and the rolls at 230°C. This produced a strip with severe lateral cracking. It appears that the billets must be heated to at least 650°C before worthwhile hot reduction can be accomplished.

The U-25 w/o Pu-6 w/o Mo alloy corroded in the hood atmosphere at temperatures above 500°C with 1500 ppm oxygen and 60 ppm water vapor in the helium. A loose black oxide was formed that brushed off easily at temperature and spalled during cooling. The atmospheric corrosion was not catastrophic, but would result in an appreciable metal loss during processing and a consequent buildup of fine oxide powder in the hood systems. It appears desirable to protect this alloy during hot working either by means of molten salt or by a high-purity atmosphere. The use of a salt coating has been tested, and less than 51 μ of carbonate salt will protect the surface during heating and rolling.

d. Evaluation of ZPR-3 SEFOR Critical Test Wafers. Present work is concerned with the evaluation of the production fuel components and completed wafers vendor-manufactured for use in SEFOR critical tests.

Fifty dummy wafers and 17 fuel wafers were inspected visually and dimensionally for conformance to the specifications. Ten additional fuel core plates were inspected visually and dimensionally, and samples from them were submitted for isotopic and spectrochemical analysis. A considerable percentage of the wafers showed evidence of poor edge-welding control as produced by electrode misalignment or poorly aligned chills. In some cases there was evidence of insufficient weld penetration. A similar condition was observed on wafers shipped to Idaho. The jackets on a small percentage of the wafers were not drawn in tightly against the core. This indicates a lack of evacuation of leakage. Contamination in excess of the specification was also found on a small percentage of the fuel plates.

4. Carbide Fuel Elements

a. Fabrication of UC-PuC Irradiation Specimens. Fifteen mixed-carbide irradiation fuel rods have been loaded by vibratory compaction.

All specimens were made by compacting a coarse fraction and infiltrating finer fractions. Ten specimens of mixed UC and PuC were assembled. The fuel charged to the specimens was calculated from the model systems and should have resulted in homogeneous fuel columns of 80% theoretical density. X radiography of the fuel columns showed void regions at the tube wall near the restrainer, indicative of low density resulting from the absence of the fine fraction at the top of the column. This condition was confirmed by autoradiography.

The low density at the top of the fuel column was caused by the deviation of the carbide system from the model. The most significant difference between the theory and practice was that the model system was made up of angular-shaped particles of malleable material while the carbides were highly brittle. The effect of the brittle nature of the fuel was to provide a wider range of particle size during settling of the matrix than was introduced into the jacket as feed. Experience gained with some rejected specimens showed that 20% of a carbide fraction could be reduced to a smaller fraction during the loading of the matrix material alone. Since the loading of the -325 mesh fraction took as much as 8 hr, a considerable attrition could be expected. Although one would not expect the generation of additional void volume by particle cleavage, a similar effect does exist.

We have previously reported that the packing efficiency of regular tetragonal shapes may be increased by rounding the edges of the particles. The increase in packing efficiency of milled particles is brought about by at least three conditions: (i) the rounding of edges reduces the surface-to-volume ratio (the particle approaches spherical dimensions); (ii) the voids in the matrix have rounded walls that reduce resistance to the entrance of the fine fraction; and (iii) extremely fine powders that result from attrition add another size fraction to the particle size distribution. Since the extent to which the carbides would be affected by abrasion is not known, it is difficult to predict the degree of this effect.

Five specimens of solid-solution (U-Pu)C were assembled in which maximum uniform density was desired. The void packing efficiency reached with these specimens was 86.7 ± 1.6%, which yields a theoretical density of 84.4 ±1.5% for the 97.5% dense particles. X radiographs and autoradiographs of the mixed-carbide specimens showed uniform density over the entire length of the fuel column. Uniform distribution of plutonium inherent in solid-solution feed materials was also confirmed by autoradiography.

One rod containing mixed carbide was made on the basis of information gleaned from the solid-solution specimens. The -325 mesh fraction was made up of 18.4% UC and 81.6% PuC, added until no additional material could be infiltrated into the UC matrix. The finished fuel rod showed no voids in the X radiograph. The total packing fraction was 86.0%,

the theoretical density 83.8%, and the plutonium carbide content 19.3%. Autoradiography revealed an area approximately 3 cm long in the center of the rod to be low in plutonium content.

5. EBR-II Test Fuel Elements

A total of 80 EBR-II test fuel rods, 16 EBR-II-type TREAT test specimens, and 3 CP-5 specimens are being fabricated. The 80 EBR-II fuel rods are of four compositions: U-10 w/o Pu-10 w/o Fz, U-15 w/o Pu-10 w/o Fz, U-15 w/o Pu-10 w/o Zr, and U-15 w/o Pu-10 w/o Ti. These compositions are being jacketed in TV-20 jacket tubes with varying sodium annuli and void volumes. Four specimens of each alloy are being fabricated for transient test in TREAT. The 3 CP-5 specimens, all of the U-15 w/o Pu-10 w/o Zr alloy, will be stainless steel jacketed to examine the compatibility of this alloy with the stainless steel under irradiation.

Four of the U-15 w/o Pu-10 w/o Ti and 4 U-15 w/o Pu-10 w/o Zr alloy fuel pins have a density 1.5 g/cc below the expected density. Radiography did not show internal porosity to account for this low density. The pins are presently being heat treated at 550°C to determine whether the low density is a result of a retained gamma-phase condition.

Assembly, welding, sodium bonding, and leak testing of the 80 EBR-II test fuel rods have been completed. The sodium bond on 49 fuel rods has passed the eddy-current inspection, and these rods have been shipped to the Engineering Irradiation Group for evaluation, encapsulation, and irradiation testing.

6. Extrusion Development

During the reporting period, (i) the large extrusion press was retooled to produce bar of 6.4 x 51-mm cross section; (ii) the temperature range at which potential ZPPR alloys can be hot worked was investigated; (iii) the degree of protection required by these alloys at the hot working temperatures was studied; and (iv) attempts were made to establish a capability of producing a single EBR-II-size pins by indirect extrusion.

E. General Fast Reactor Fuel Reprocessing Development

1. Skull Reclamation Process

Pilot-plant studies on a scale of 1.5 kg of uranium are essentially complete. The development of plant-size (~4.25 kg U) remotely operated equipment is underway.

The modifications in the alternative flowsheet (see Progress Report for June 1965, ANL-7071, p. 24) occur in the step following the noble-metal-extraction step, an early step in both flowsheets and are as follows: uranium

oxide suspended in the molten salt phase is reduced with a 60 w/o Mg-Zn solution, and the metallic uranium precipitates in the reducing alloy. After the reduction is complete, both the Mg-Zn solution and the flux are discarded as waste. The precipitated uranium is redissolved in a Zn-14 w/o Mg solution and the product solution is transferred to the retorting operation.

Five pilot-plant runs recently completed on the basis of the alternative did not yield any operational difficulties. The elapsed operating time for a run with the alternative flowsheet was about 10 hr as compared to about 18 hr for the previous flowsheet. Preliminary analytical results were highly encouraging. Uranium losses were low, about 2%, and fission product-decontamination factors were similar to those obtained in pilot-scale runs with the previous flowsheet. Additional pilot-plant demonstrations of the alternative flowsheet are not presently planned. Additional development work on this process is now being conducted in plant-prototype skull-reclamation equipment (see ANL-7071, p. 25).

2. Pyrochemical Processes

Compact, pyrochemical processes are under development for processing fast breeder reactor fuels of the ceramic (e.g., oxide and carbide) or metallic types.

In the development of cadmium-based processes for the recovery of uranium-plutonium fuels, liquid metal-molten salt extraction procedures are used for the separation of uranium, plutonium, and fission products (see Progress Reports for March 1965, ANL-7028, p. 31, and for June 1965, ANL-7071, p. 27). Two systems are being considered for use as the liquid metal phase: 85 a/o Cd-15 a/o Mg, and 70 a/o Cd-15 a/o Mg-15 a/o Zn. Information on solubilities of plutonium, uranium, and fission products in process solvents, corrosion of candidate materials of construction, stability of uranium and plutonium solutions, distribution coefficients of fuel constituents between liquid metals and molten salts, and other physical properties of pertinent systems is being reviewed and extended to determine which of the two solvents should be selected for further process-development studies.

An alternative process concept utilizes separations based on the partition of uranium, plutonium, and fission products between Cu-10 w/o Mg and different Zn-Mg alloys in mutual contact with molten NaCl-KCl-$MgCl_2$. Existing distribution-coefficient data indicate that alkali metal, alkaline earth, and lanthanon fission products will be transferred to the salt, plutonium to a Zn-3 w/o Mg alloy, uranium to a Zn-80 w/o Mg alloy, and the noble and refractory metal fission products to Mg-10 w/o Cu alloy. Experiments are underway to test the chemical feasibility of this type of separation.

A supporting program to determine the corrosion resistance of ferrous alloys to copper-magnesium/chloride salt systems is in progress. A screening test for corrosion resistance of the following alloys was

conducted: mild steel, 1% Cr alloy steel, Type 304 stainless steel, and Type 405 stainless steel. Specimens of these alloys were exposed to Cu-Mg/$MgCl_2$-NaCl-KCl melts for 200 hr at 600°C and at 800°C (purified chloride salts were used in this test). Preliminary results indicate that the ferrous alloys are promising container materials for the systems tested. In copper alloys containing from 10 to 50 w/o magnesium, the corrosion was generally within 0.1 to 1.0 mil for the 200-hr exposure at 600°C and at 800°C.

Since Zn-Mg alloys are used in various liquid metal processes, solubilities of container material constituents and fission products in these alloys and their constituent elements are of interest. The following solubilities of iron, niobium, zirconium, and chromium at 800°C were obtained during measurements of distribution coefficients:

	Solubility (w/o) in		
	100 w/o Zn	50 w/o Zn-50 w/o Mg	100 w/o Mg
Iron	7.7	0.2	0.075
Niobium	3.0	0.04	<0.0001
Zirconium	12	0.95	0.64
Chromium	1.5	0.08	~0.045

Engineering work related to the development of continuous molten metal-molten salt extraction processes (see Progress Report for February 1965, ANL-7017, p. 37, and March 1965, ANL-7028, p. 31) is underway in the following areas:

a. Component Test Loop. A simple test loop is being assembled to gain experience in circulating molten $MgCl_2$-based salts. A centrifugal pump, previously successfully demonstrated at Oak Ridge National Laboratory for circulation of Molten Salt Reactor Experiment molten fluoride salt, has been obtained for installation in the test loop.

b. Salt Purification Facility. An engineering-scale facility has been constructed for purification of large batches (50 kg) of molten chloride ($MgCl_2$-NaCl-KCl) salt. Untreated salts containing $MgCl_2$ are extremely corrosive toward all steels and contain large quantities of insolubles and substances (particularly water) that react with UCl_3 to form UO_2Cl_2 and UO_2. The impure chloride salt mixture is purified by contact with a Cd-Mg alloy at 550-600°C and then filtering at temperatures between 450 and 500°C through a stainless steel filter having 20-μ pores. The first batch of salt has been purified in the facility. Analytical results showed that the purified salt mixture contained 0.26 w/o oxygen (as MgO), which is about that expected for a first batch of salt that has been filtered through a new filter. Previous work has shown that the purity of the salt increases with continued use of a filter because of the buildup of an effective filter cake on the filter. This work indicated that an order of magnitude decrease in oxygen content occurs after the first use of the filter.

II. GENERAL REACTOR TECHNOLOGY

A. Experimental Reactor and Nuclear Physics

1. Calibration of Neutron Sources with Mn^{56}

Absolute and relative calibrations of neutron sources as well as experiments rely heavily on the manganese bath technique, a method of moderating fast neutrons, capturing them in manganese, and then counting the Mn^{56} activity. Since only 30 or 40% of the original neutrons are absorbed by manganese for concentrations of 0.2 to 0.4 kg/liter $MnSO_4$ in H_2O, it is essential to have an accurate knowledge of the actual atom ratio of manganese to hydrogen. This is also fundamental for evaluation of the effective manganese-to-hydrogen cross-section ratio by variation of the concentration with constant source strength.[1] Our experience with various methods of chemical analysis and dehydration has led to the following technique, which reduces the problem to a simple gravimetric and volumetric measurement made at a constant temperature.

Powder is taken from an unopened bottle of ACS-grade manganese sulfate monohydrate and is quickly put in a bottle, which is then closed and rapidly weighed. The salt is dissolved with a small amount of H_2SO_4 and H_2O_2 in H_2O in a previously calibrated volumetric flask. This basic high concentration is subsequently used as a source for making dilute solutions in the same flask.

To obtain the exact initial hydrogen content of the monohydrate, powder from the original bottle is weighed, gently evaporated to dryness at 300°C, occasionally pulverized, and brought to constant weight. The water content of material taken from two different bottles is about 1% greater than the water of hydration.

Results are presented in Figures 9 and 10. Reproducibility was better than 0.1%. Additional points are plotted representing information obtained from other sources.[2-4]

A least-squares fit to a polynomial of five or six terms offers the best agreement with our data. If ρ is the density (in kg solution/liter solution) at 30.0°C, then the concentration C_m (in kg $MnSO_4$/kg solution)

---

[1] De Volpi, A., and Porges, K. G., ANL-6797 (1963).

[2] Gerlach, G. T., Zeit. Anal. Chem. 28, 478 (1889).

[3] Handbook of Chemistry and Physics (1959) (Chemical Rubber Publishing Co., Cleveland, Ohio).

[4] Reeder, S. D., Private Communication (1964).

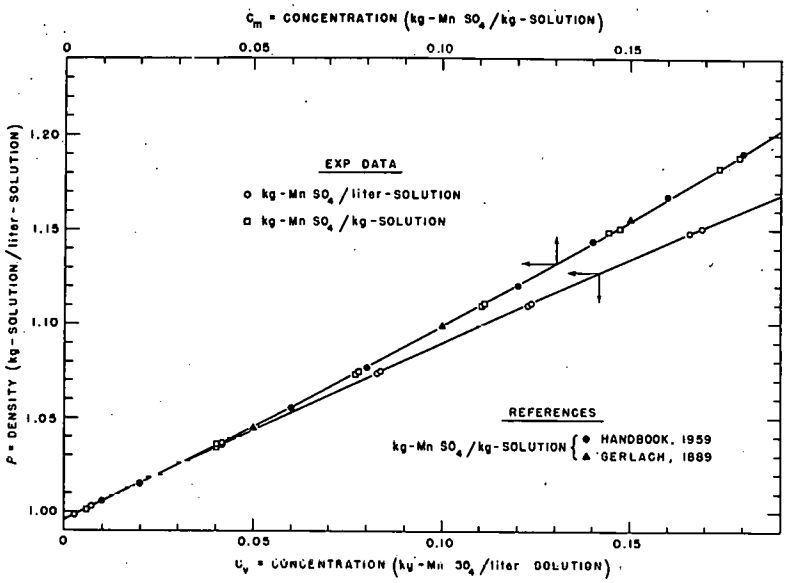

Figure 9. Volume and Weight Concentrations of Aqueous $MnSO_4$ Solution in the Density Range from 1.00 to 1.20 kg/liter. The curves drawn through the points are the least-squares polynomials given in Eqs. (1) and (2). (Neg. No. 112-4684).

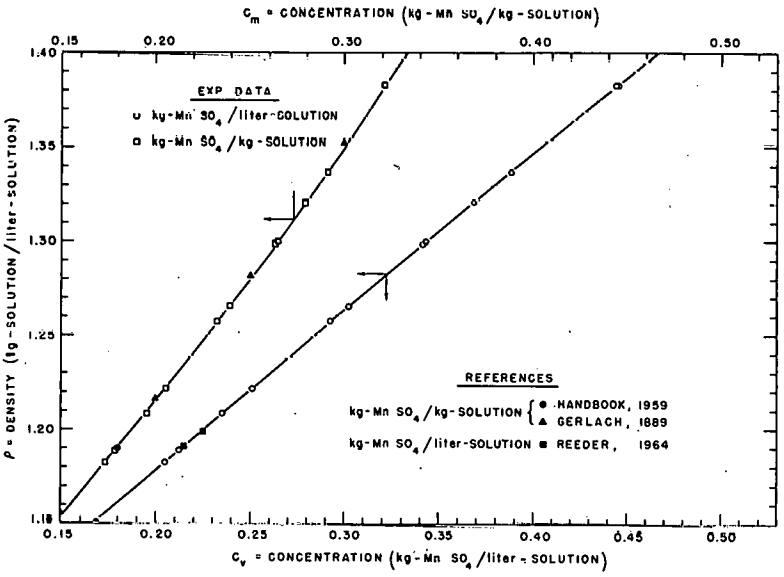

Figure 10. Volume and Weight Concentrations of Aqueous $MnSO_4$ Solution in the Density Range from 1.15 to 1.40 kg/liter. The curves drawn through the points are the least-squares polynomials given in Eqs. (1) and (2), (Neg. No. 112-4685).

and C_v (in kg $MnSO_4$/liter solution) at that temperature are given by

$$C_m = -1.4088 + 1.4227\,\rho + 0.56713\,\rho^2 - 0.77726\,\rho^3 + 0.20073\,\rho^4 \quad (1)$$

and

$$C_v = 0.17697 - 2.0400\,\rho + 2.1603\,\rho^3 + 0.33622\,\rho^3 - 0.89290\,\rho^4 + 0.26374\,\rho^5. \quad (2)$$

B. Theoretical Reactor Physics

1. Epicadmium Capture-to-Fission Ratios of Pu^{239} and Pu^{241}

A study has been made of methods that may be used for the determination of capture-to-fission ratios of Pu^{239} and Pu^{241} in the epicadmium energy range. These methods involve the irradiation of thin foils (or capsules), followed by a combination of mass-spectrographic, radiochemical, and chemical analysis.

a. First Method: Short Epicadmium Irradiation followed by Radiochemical and Mass-spectroscopic Analysis. The first method is similar to that used in EBR-I experimental studies,[5] except that the foils are covered with cadmium. An irradiation period of about 30 days at 40-MW power level ($\tau = \phi_{epi} t \simeq 6 \times 10^{20}$) is satisfactory. The value of α^{49}_{epi} is given by

$$\alpha^{49}_{epi} \simeq \frac{\Delta N^{40}_{(\tau)} / N^{49}_{(\tau)}\; N^{49}_{(\tau)} (1 - \sigma' \tau)_{epi}}{N^{137}_{(\tau)} / Y^{137}}, \quad (1)$$

where

α^{49}_{epi} = epithermal capture-to-fission ratio of Pu^{239};

Y^{137} = fission yield of Cs^{137};

$N^{137}_{(\tau)}$ = isotope abundance of Cs^{137} at exposure τ;

$N^{49}_{(\tau)}$ = isotope abundance of Pu^{239} at exposure τ;

$N^{40}_{(\tau)}$ = isotope abundance of Pu^{240} at exposure τ;

---

[5] Crouthamel, C. E., Stupegia, D. C., and Stevens, C. M., Nucl. Sci. Eng. 21, 179 (1965).

$$\Delta N^{40}_{(\tau)} = N^{40}(\tau) - N^{40}(0);$$

$$\tau = \phi \times \text{time};$$

$$\sigma' = (\sigma^{49}_a + \sigma^{40}_a)/2!;$$

and $\sigma'\tau$ is a small correction term.

The concentration of Cs^{137} is found by radiochemical analysis, while the change in the Pu^{240} concentration, ΔN^{40}, and the Pu^{239} concentration are determined by mass-spectroscopic and chemical analysis.

The maximum possible error in the value of α^{49}_{epi} given by Eq. (1) is ~9.5%. The largest contribution to this calculated error is that due to the uncertainty in the value of fission yield Y^{137} of Cs^{137} (~7%). According to some measurements,[6] this uncertainty may be appreciably smaller than 7%.

b. Second Method: Determination of the Epithermal Value of α in Terms of Thermal Values. The second method, involving the irradiation of foils with and without cadmium covers,[7] eliminates any need for the fission-yield term Y^{137}. The value of α^{49}_{epi} is given by

$$\alpha^{49}_{epi} = \left[\frac{(N^{137}/N^{137}_{epi}) - 1}{(N^{40}/N^{40}_{epi}) - 1}\right]\left[\frac{1 - (\sigma'\tau)_{th}}{(1 - \sigma'\tau)_{epi}}\right]\alpha^{49}_{th}. \qquad (2)$$

The maximum error is ~7%. The error due to uncertainty of α^{49}_{th} is assumed to be 1.5%.

c. Third Method: Dual Irradiation. The third method involves the irradiation of two sets of cadmium-covered plutonium foils, one for a long exposure (τ') and one for a short exposure (τ). This method eliminates the need for radiochemical analysis. The value of α^{49}_{epi} is given by

$$\alpha^{49}_{epi} = \frac{\left(C_0(\Delta N^{40}_{(\tau')}/N^{49}_0\right)}{\left[2\Delta N^{49}_{(\tau)}/\left(N^{49}_0 + N^{49}_{(\tau)}\right)\right] - C_0\Delta N^{40}_{(\tau')}/N^{49}_0}, \qquad (3)$$

where $C_0 = \tau/\tau'$ and $\tau' = \phi t \simeq 5.8 \times 10^{20}$ not for foils with short burnup. The value of C_0 is determined with the aid of irradiated foils of cobalt.

---

[6] Katcoff, S., Nucleonics, 18(11), 201 (1960).

[7] Conway, D. E., Cook, H. D., and Gunst, S. B., Nucl. Sci. Eng. 22, 20 (1965).

For a reasonably accurate determination of α^{49}_{epi}, it is required that burnup of Pu^{239} be appreciable. Values of maximum error are given below for different values of "τ:"

Irradiation Time in EBWR...	336	493	644
$\tau = \phi t$ (nvt)	6.5×10^{21}	9.6×10^{21}	1.26×10^{22}
$\delta\alpha^{49}_{epi}/\alpha^{49}_{epi}$(%)	14	7.7	5.7

It appears from the above analysis that short-term irradiation (~30 and 60 days) of foils, with and without cadmium covers, should yield values of α^{49}_{epi} and a check of Y^{137}, by the application of the first two methods. An additional long-term irradiation of cadmium-covered foil should also yield α^{49}_{epi}.

d. α^{49} in Fuel Elements Compared with α^{49} in Coolant-Moderator. The placement of test foils in a U-tube in EBWR could smooth out resonance effects on the flux in the fuel elements. To evaluate these effects, the value of α^{49} in the coolant was compared with the value of α^{49} on the surface of fuel elements in the EBWR Plutonium Recycle Experiment. The latter values were evaluated with the aid of the RIFF-RAFF[8] code, with 5800 groups spanning the energy range from 0.532 to 85.5 eV, and allowing for interference effects of U^{238} and U^{235} in this range. The results of the calculation indicated: α^{49}_{epi} in coolant is 11% and 15% lower than corresponding values of α^{49}_{epi} on the surface of a 1.5% enriched Pu^{239}, and 6% enriched U^{235} foil element, respectively.

2. ZPR-7 Data Analysis

Parameters previously obtained (see Progress Report for May 1965, ANL-7046, pp. 43-44) from THERMOS problems and from three-group GAM-I problems using Hanford cross sections for U^{235} and U^{238}, were used to calculate various quantities for all the Hi-C and BORAX-V uniform lattices studied in ZPR-7. Among the quantities calculated were radial reflector savings, U^{238} to U^{235} fission ratio (δ^{28}), initial conversion ratio, and the ratio of capture to fissions in U^{235} (α^{25}). Agreement between theory and experiment was rather good for reflector savings and α^{25}. Calculated initial conversion ratios were usually higher than experimental, especially for the looser lattices. In the case of δ^{28}, agreement was not good, as experimental values were considerably higher than theoretical ones.

Heterogeneous effects in the fast-fission range were investigated and found to be small. It is believed that the disagreement between theory and experiment on δ^{28} is primarily a result of inadequacies in the cross-section data.

[8] Kier, P. H., "RIFF-RAFF, A Program for Computation of Resonance Integrals in a Two-region Cell," ANL-7033 (May 1965).

C. High-temperature Materials

1. Ceramic Fuel Materials

a. (Th-U-Pu) Sulfides. Experiments were begun on the oxidation of uranium monosulfide wherein a gas chromatograph detector was used for measurement of reaction rate. The results of calibration tests and preliminary oxidation runs indicate that the chromatograph is operating satisfactorily.

Several runs were made with US pellets at 700°C in an atmosphere of helium containing 0.375 v/o oxygen. Part of the outer oxide layer on a sample that was exposed for 2 hr powdered and fell off during the run. Analysis of the gaseous reaction products revealed a considerable amount of SO_2. Previously reported results indicate that α-US_2 also is a reaction product.

Additional experiments are planned to more completely identify reaction products and better characterize the oxidation process.

b. (Th-U-Pu) Phosphides. Studies have continued of the resistance of uranium monophosphide to corrosion by various media. Although UP powder exhibited virtually no weight change after being immersed in boiling water for 2 hr, chemical analysis showed a measurable oxygen pickup. For example, one sample, which had an original oxygen content of 0.13%, showed an increase to 0.32% after two hours in boiling water. Relatively pure UP powder (containing 0.06% oxygen) exhibited an increase in oxygen content to 0.09% on standing in air for one day and a further increase to 0.12% on exposure to air at room temperature for five additional days. Similar powder showed little reaction with concentrated phosphoric acid at room temperature but reacted violently with hot H_3PO_4. The resulting solution was green, indicating that the uranium was oxidized to the tetravalent state.

A series of tests is being conducted to determine flexural strength of the composition 38 w/o uranium phosphide-62 w/o uranium dioxide at various temperatures. Specimens were made by ball milling the 38 w/o UP-62 w/o UO_2 for 5 hr in xylene, adding 1 w/o of stearic acid as a binder, and dry pressing the mixture. Because of laminations, the pressure was lowered to 700 kg/cm^2 to produce sound specimens. The bars formed, 6.4 mm wide by 57 mm long and slightly less than 6.4 mm in thickness, were fired in vacuum at 1900°C for 2 hr and had an average density of 97% of the theoretical value.

c. Anelasticity of Some Uranium Compounds. Additional data on the effect of the oxygen content on the elastic modulus of uranium

oxides are shown in Figure 11. Specimens with two different grain sizes were tested, and apparently this factor did not have bearing upon the elastic modulus.[9] Figure 11 suggests that a change in the oxidation mechanism occurred when the O/U ratio reached a value of about 2.06.

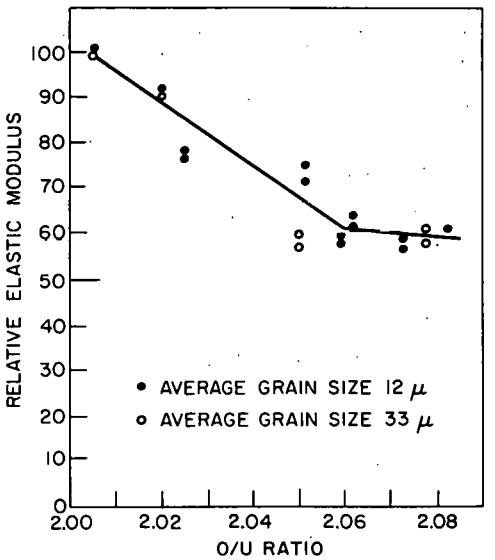

Figure 11

Effect of O/U Ratio on the Elastic Modulus of Uranium Oxide at Room Temperature

In order to elucidate this point metallographic studies of the specimens with a grain size of 12 γ were performed. The microstructure of a sample with O/U ratio of 2.027 showed a marked contrast with that of a specimen with O/U ratio of 2.005. Cracks had propagated along the grain boundaries, and a considerable amount of etch pits had appeared in the center of the grains. A second phase with a needle-like shape was detected. According to the phase diagram of Gronvold[10] this must be U_4O_9, which had precipitated upon cooling. The second phase was concentrated near the surface, indicating that there was an oxidation gradient. A sample with an O/U ratio of 2.051 showed extensive cracking and etch pits, and the second phase was more uniformly distributed. In specimens with O/U ratio between 2.06 and 2.082 the amount of cracks and etch pits remained invariable with respect to the sample of O/U ratio of 2.051. The amount of second phase increased as the O/U ratio became larger.

Comparison of the elastic and metallographic studies performed up to the present suggests that a probable cause of the large decrease of the Young's Modulus on the first stages of the oxidation might have been due, to a large degree, to the cracks originated by the stresses introduced by the diffusion of oxygen into the body.

---

[9]The elastic modulus was determined by a sonic method.

[10]Gronvold, F., High-temperature X-ray Study of Uranium Oxides in the UO_2-U_3O_8 Region, J. Inorg. Nuclear Chem., 1, 357-370 (1955).

Apparatus for the determination of the elastic modulus and internal friction as a function of temperature is being erected. The main problem encountered has been that leaks around the electrodes have made it difficult to obtain a good vacuum.

d. Uranium-mixed-anion Systems. Phase equilibrium in the system UC_2-US is being investigated as a necessary adjunct to the study of the system UC-US. One-phase UC is difficult to make, and the hyper-stoichiometric material almost always contains UC_2. Consequently, any practical application of the UC-US system would require a knowledge of reactions in the system UC_2-US. This system most likely is not a true binary.

Compositions of UC_2-10 w/o US, -25 w/o US, -50 w/o US, and -75 w/o US were mixed by ball milling in xylene and dry-pressed specimens were equilibrated in vacuum at 1600°C for 4 hr. Examination by X-ray diffraction showed that reflections for US were absent from all patterns except for UC_2-75 w/o US. Apparently US is soluble in UC_2 up to 50 w/o US. The tetragonal structure of the UC_2 is expanded in the "a" direction with the solution of US, and the "c" dimension remains constant.

New determinations of the liquidus curve in the UP-US system show a maximum melting point at approximately UP-30% US, confirming earlier results. The existence of a melting-point maximum is unusual, but not unique. Similar maxima have been observed in the systems UC-US and PuO_2-UO_2. However, a satisfactory explanation for the occurrence of this phenomenon has not as yet been advanced.

2. Liquid-Metal Corrosion

a. Polarization Studies. The temperature of oxygenated sodium in the polarization cell has been reduced to 400°C to avoid the previously reported difficulty attributed to absorption of surface film oxygen by underlying zirconium sample metal (see Progress Report for May 1965, ANL-7046, p. 49). Although this problem appears to have been eliminated sufficiently, test runs with zirconium electrodes polarized anodically in the 400°C (central temperature) sodium have produced sample-surface films having numerous metallic spots of the sort previously correlated with moisture impurity. Whether the effect is inherently more severe at this temperature or was due to an excessive moisture level for this particular experiment is being determined.

A rod sample of TV-20 was exposed for about 21 hr to highly oxygenated sodium at 540°C to determine its suitability as a polarization test specimen. The sample lost weight (about 1 mg/cm^2), and no surface film suitable to low current polarization studies was evident. A number of spot blemishes similar to those associated with moisture impurity were observed.

Of incidental interest is an effect seen when fresh sodium is initially combined with Na_2O_2, prior to tests, to produce oxygenated sodium. Normally, 145 g of sodium and 4 g of Na_2O_2 are heated together in argon to produce sodium containing near-saturation concentrations of (presumably) Na_2O at the test temperatures. During heating, the reaction with fresh sodium is occasionally quite vigorous, sometimes audible, and on occasion has caused loss of sodium past the O-ring gas seals of the cell cover. A cover clamp has been added to prevent the leakage of sodium. No air fire has occurred with escaped, initially molten sodium.

b. Lithium Corrosion Studies at Elevated Temperatures. One tantalum alloy (Ta-8.5 w/o W-2.5 w/o Hf), one molybdenum alloy (Mo-30 w/o W), and unalloyed specimens of tantalum and molybdenum were exposed to lithium for 8.5 days at 1200°C under slightly positive, inert-atmospheric pressure. Alloys (and test lithium) were contained in unalloyed capsules of their respective base materials.

Metallographic examination revealed that the Mo-30 w/o W alloy had experienced no attack and no change in microstructure during corrosion testing. There was no evidence of corrosion of the molybdenum capsule along its interior walls. However, a slight intergranular attack was detected on the bottom interior surface. No change in weight of the alloy insert was observed.

The Ta-8.5 w/o W-2.5 w/o Hf alloy suffered no corrosion attack during the test. Some fabrication (rolling) effects were still apparent after the test. Corrosion penetration was found to be rather severe at the bottom interior surface of the tantalum capsule. There were no significant weight changes for either tantalum alloy specimens. However, considerable penetration was noted in the case of unalloyed tantalum.

The three heat-zone assemblies and power supplies for high-temperature liquid-metal-corrosion studies have been received. The installation of this equipment in the vacuum chamber is now in progress.

3. Component Surveillance Loop

A loop designed to test the effects of 1200°F sodium on engineering-size samples and components is about 80% complete. Delivery is expected approximately by August 15, 1965.

The sodium tank has been welded and is now being leak tested and dye checked. Construction of the loop will proceed as soon as the tank is delivered.

A continuous oxygen-analysis meter has been received. The entire assembly of water- and oxygen-analysis equipment has been mounted in a console for attachment to the loop when it is made operational. The assembly of the initial wear-testing device to be used in the loop is largely completed. A number of refinements of the loading apparatus are in fabrication. This unit will be assembled for pot testing as soon as all of the needed components are received.

Dimensional analysis of the parameters included in wear testing of materials resulted in the development of a function which will be used to correlate the results of the wear-testing studies.

4. Irradiation Testing

a. Vibratorily Compacted UC-PuC. The postirradiation examination of specimens from capsule ANL-56-7 was begun. Four specimens are vibratorily compacted, physically mixed powders of UC-20 w/o PuC, and two are vibratorily compacted PuC powder. The specimens were compacted to ~80% of theoretical density. The fuel is 3.9 mm in diameter and 51 mm in length. Overall specimen length is 82 mm. The cladding materials are either Nb-1 w/o Zr or Type 304 stainless steel, both 0.23 mm thick. Maximum cladding surface temperatures ranged from 550 to 675°C at heat ratings of 169 to 212 W/cm. Estimated burnup ranged from 5.3 to 6.8 a/o metal atoms (1.4×10^{21} to 1.8×10^{21} fiss/cc). A summary of the irradiation conditions and the postirradiation examination to date is given in Table XI.

Table XI Irradiation Summary for Capsule ANL-56-7

Specimen No.	Fuel	Cladding	C in PuC, w/o	Estimated Burnup a/o	Estimated Burnup Fiss/cc x 10^{21}	Linear Heat Rating, W/cm Avg	Linear Heat Rating, W/cm Max	Clad Surface Temp, °C Avg	Clad Surface Temp, °C Max	Max %Δ Dia	%Δ L	%Δ Vol
C-43	PuC	Nb-1 w/o Zr	4.24	5.3	1.4	167	169	510	550	0.1	Neg.	0.3
F-8	PuC	304 SS	4.24	6.0	1.6	196	212	605	675	14.3	2.0	-
F-19	UC-20 w/o PuC	304 SS	5.10	5.8	1.5	171	178	525	570	2.8	0.3	3.5
F-20	UC-20 w/o PuC	304 SS	4.76	6.8	1.8	194	205	600	645	4.7	1.3	7.3
C-72	UC-20 w/o PuC	Nb-1 w/o Zr	5.10	6.8	1.8	188	194	575	635	0.2	Neg.	0.4
C-70	UC-20 w/o PuC	Nb-1 w/o Zr	4.74	6.8	1.8	196	199	600	650	0.4	Neg.	0.5

None of the mixed-carbide specimens failed. The specimens in Nb-1 w/o Zr alloy cladding showed negligible changes in dimensions. The maximum volume change as measured by liquid displacement was 0.5%. The stainless steel-clad mixed-carbide specimens showed larger volume changes, the magnitude of which depended upon burnup and heat rating. A maximum diametral change of 7.3% was observed, indicating that the stainless steel still possessed a high level of ductility.

The PuC specimen jacketed with Nb-1 w/o Zr alloy was also intact. The stainless steel-jacketed specimen showed a clad rupture near the top of the fuel section after a maximum diameter increase of 14.3%, thus indicating to a greater degree the retention of ductile properties of the stainless steel. The fuel showing through the split appeared to be massive and not powdery. Swelling was restricted to the fuel section and was accompanied by a double bowing of the specimen. The bowing was caused by axial fuel expansion and external restraint on the specimen.

D. Other Reactor Fuels and Materials Development

1. Nondestructive Testing

a. Ultrasonic Instrument and Transducer Development. A Schlieren system for observing pulsed ultrasonic waves is being assembled. The system is similar to the continuous-wave Schlieren system utilized earlier in transducer-probe studies. The pulsed system, however, will contain a light source, EG & G flashtube FX-31, which is synchronized with the pulse generator. The required electronic circuitry is under construction.

b. Development of a Neutron-image Intensification System. The image-intensifier tests conducted with the Cm-Be neutron sources have been completed. The 12 sources had a total fast-neutron yield of about 6×10^9 neutrons/sec at the time of the imaging tests. The moderator tank, made for neutron activation studies, was used in the initial tests. The twelve sources were arranged in a water-filled tank around a central tube. The moderated neutron beam from the central tube was collimated by two boral sheets, each containing a 2.5-cm-dia hole, and the neutron beam was detected by the image intensifier. For ease of manipulation the intensifier and collimators were positioned below the moderator tank.

The height and radial positions of the sources were approximately optimized as indicated by a BF_3 counter. The neutron image was not detected with the closed-circuit vidicon television system (f/2.0 lens), but was detectable visually by using a mirror system to view the output phosphor of the intensifier tube. The neutron intensity under these circumstances, as determined by gold foil irradiations, was 1.53×10^5 total neutrons/cm^2-sec with a cadmium ratio (1/2-mm-thick cadmium cover) of 2.3. The thermal neutron intensity was, therefore, about 8×10^4 n/cm^2-sec. This neutron intensity would be expected, from previous measurements at the reactor, to be visually detectable by use of the intensifier but not detectable by use of the vidicon television system. The collimation of the neutron beam was poor, but gross objects could be shadowed.

The sources were then arranged in a glass water tank and the beam was taken directly from the bottom of the tank below the sources.

The neutron intensity was significantly improved, and the optimum position of the sources within the moderator tank could easily be determined by visual observation of the intensifier-output phosphor. The total neutron beam intensity was 2.55×10^5 n/cm^2-sec with a cadmium ratio of about one. Images were detectable with the television system, but the need for improved collimation was still apparent.

The tests indicate that fast-neutron yields of the order of 10^{11} neutrons/sec or more will be necessary in order to provide a useful neutron beam for imaging applications.

c. Infrared Systems for Nondestructive Testing. Preliminary tests were performed to determine the optimum detector delay time and fuel-sample velocity. The sample used was a 1.4-mm aluminum-clad flat fuel plate with known defects. The surface of the sample under inspection was coated flat black to provide uniform absorption and emission of radiant energy. The detector spot was focused at various distances from the heat line, and the scans were made at various velocities.

The best test results to date have been obtained with heat and detector spot separation of 2.5 cm. The scan speed was experimentally determined to be 4 cm/sec. Because of strong stray radiation from the heat source entering the radiometer, a heat detector spot time separation less than one second was unobtainable. A light shield will be installed to obtain heater-detector spot separation of one second or less.

Work on an infrared heat source has been renewed. A 1000-W, 115-V projection lamp (Sylvania Type CTS) is now used for the heat source. The reflector is a 172-mm-dia, 98-mm-focal-length, first-surface mirror. The projected size of the filament is 6 x 6 cm.

E. Engineering Development

1. Two-phase Flow

a. Void Fraction--Pressure-drop Facility. This facility is still inoperative pending completion of repairs.

2. Boiling Liquid Metal Technology

a. Niobium-1% Zirconium Loop. Construction is complete and the loop was crated for shipment. The final inspection and leak-check were made at this time and witnessed by ANL staff. The well X-rays have been received and will be reviewed before final acceptance of the loop assembly.

The loop-support structure assembly, heater and preheater units, and the reflector and balancing assemblies are 95% complete and delivered, with the exception of the tantalum components. Vendor delays have caused an overall delay in schedule of 12 weeks.

The clean assembly room required for housing the Nb-1% Zr loop until it is placed in the vacuum chamber is under construction.

Instrumentation procurement and assembly are in progress. The chromel-alumel thermocouples will be delivered in early August. The pressure transducers and oven are complete and ready for installation. The NaK cooling system for the electromagnetic flowmeters is nearly complete. The argon- and sodium-purification systems are being fabricated. Bids for the residual gas analyzer have been received and are being evaluated.

The data-acquisition system has been delivered, and the computer routines for data analysis are under study.

The vacuum system was operated for considerable periods of time. Overnight, unattended operation of the pumping system, the liquid nitrogen system, and the chamber oven is feasible. The chamber was baked extensively and vacuum levels in the 10^{-9}-Torr region were obtained. The chamber bakeout revealed an insufficient heater capacity for the base of the chamber and that some contamination of the ion gauge probably occurs when the liquid nitrogen trap is inoperative for long periods. The system was shut down preparatory to installing additional heaters and thermocouples and for conversion to a two-zone heater-control system. An operating manual for this equipment is being written.

b. Heater Experiments

(i) Thermal Radiation Heater Experiment. This experiment has been terminated and a topical report is forthcoming.

(ii) Electron Bombardment Heater Experiment. The new power leads have been installed, and the vacuum system has been reworked to provide a pressure of 4×10^{-7} Torr. After degassing, this sodium pool-boiler will be brought back up to temperature to test the new design.

3. General Heat Transfer

a. Heat Transfer in Double-pipe Heat Exchangers

(i) Countercurrent Flow. Initial programming of the present formulation of the countercurrent-flow heat-exchanger problem for exploratory computations with the CDC-3600 has been essentially completed,

and "debugging" is in progress. The formulation applies to turbulent liquid-metal heat exchange in a concentric-tube exchanger with a narrow annular space, and will determine both fully developed heat transfer coefficients and the new design factor called the "Effectiveness Coefficient." A heat-exchanger configuration of adjacent parallel plane channels has also received consideration.

(ii) Cocurrent Laminar Flow. Computations related to the general problem of cocurrent laminar flow in a concentric-tube exchanger have been completed (see Progress Report for March 1965, ANL-7028, p. 58). Because of time limitations specified for this problem, together with the usual difficulties encountered in the use of new equipment, the original plans to make full use of the hybrid (analog/digital) computing facilities were not followed. Valuable experience in the use of such equipment, however, was obtained.

b. Heat Transfer in Liquid-metal-cooled Reactor Channels

(i) Nonuniform Heat Flux. A new research topic, as formally proposed for FY 1966, was begun this month. This topic relates to the investigation of new methods for the prediction of temperatures in liquid-metal-cooled reactor channels with nonuniform heat-flux distributions. These methods do not rely upon the traditional use of heat transfer coefficients, but introduce "higher ordered" coefficients which are independent of the flux distribution, and, when accuracy is desired, offer computational procedures which are potentially more convenient than traditional methods. Computation of various quantities related to the determination of these "higher ordered" coefficients was assigned as a problem for three graduate students in the AMU-ANL Summer Engineering Practice School. These computations have been completed for a parallel plane channel over a Prandtl number range from 0.003 to 0.03, and for Reynolds numbers up to 10^6.

4. Electric Master-Slave Manipulator Mark E4

One slave arm is about 85% complete. The remaining components to be fabricated consist of the support structure, some of the gears for the arm motions, three gear housings, and the cooling system. The master arm for this unit is about 35% complete.

5. Advanced Component Designs

a. Cup-rotor Motor. A detailed study has been made of the interrelationship of the significant design parameters of two-phase, 60-cycle, cup-type servo motors. Motors of this type are suitable for use with electric master-slave manipulators of 50- to 200-lb load capacity. This type of motor has been shown to have a much higher torque-to-inertia

ratio than the squirrel-cage servo motors. The cup-rotor motor can have an effective inertia which is less than 3% of the maximum load of the manipulator. At the present state of development, this is adequately low compared to the inertia of the manipulator arm.

b. Higher-force Feedback Studies. Studies have been carried out of methods to obtain higher static and dynamic force feedback for electric master-slave manipulators. We believe that the frequency response in the forward direction, i.e., from master to slave, need be only about 5-10 cps, but that the feedback from slave to master should be much higher. A breadboard model has been started, utilizing a 60-cycle motor for the slave side and a 400-cycle motor having a high torque-to-inertia ratio for the master side.

F. Chemical Separations

1. Fluidization and Volatility Processes

a. Recovery of Uranium and Plutonium from Low-enrichment Fuels

(i) Laboratory Support Work. Experimental evaluation of bromine pentafluoride as a selective fluorinating agent for uranium in uranium-plutonium fuel materials was continued (see Progress Report for June 1965, ANL-7071, p. 44). Consideration for the use of BrF_5 is based on the fact that the reaction between BrF_5 and mixtures of uranium and plutonium compounds results in the conversion of uranium to volatile UF_6 while plutonium is converted to nonvolatile PuF_4. Plutonium is recovered as PuF_6 in a subsequent step by the fluorination of PuF_4 with fluorine.

A series of tests was performed to determine the extent of plutonium volatility during the reaction of U_3O_8 with BrF_5 and the effect of this reaction on the subsequent fluorination of plutonium with fluorine. In each of two tests, a reaction mixture containing 5.8 g U_3O_8, 0.2 g PuO_2, 0.07 g fission product oxides, and 10 g alumina was contacted with a gas phase containing 20 v/o BrF_5 in nitrogen for 1 hr at 400°C. The volatile reaction products and excess BrF_5 were passed through a trap containing soda-lime, which was subsequently analyzed for plutonium. The residue remaining after the BrF_5 step was treated in flowing 100% fluorine at 550°C for a reaction time of 5 or 8 hr. The plutonium concentrations of the alumina bed after reaction with fluorine were 0.038 w/o after 5 hr and 0.011 w/o after 8 hr. These concentrations correspond to removals of 97.9 and 99.5% of the plutonium in the reactant mixture. Greater than 99% of the uranium present in the reactant mixture was removed during the combined fluorination steps. These results showed that the BrF_5 fluorination step had no harmful effect on the plutonium-removal step.

Analysis of the soda-lime from the trap indicated that none of the plutonium had been volatilized during the BrF_5 fluorination step. The nonvolatile character of the plutonium product was verified in an additional test in which 2 g PuO_2 was reacted with BrF_5 for 1 hr at 400°C. Results of the tests thus far indicate that quantitative separation of uranium and plutonium is possible by this method.

(ii) Decladding and Fluorination. Development studies are being performed in a 6-in.-dia fluid-bed reactor to evaluate the decladding of Zircaloy-2-clad UO_2 fuel bundles with HCl. A series of tests simulating decladding conditions were performed to determine: (1) the effect on the oxide fuel of small concentrations of oxygen in the decladding reagents, and (2) the efficiency of packed beds of alumina in filtering U_3O_8 fines generated by the reaction between oxygen (in small concentrations) and the UO_2 fuel.

In three of the tests, the operating procedure consisted of charging a quantity (about 12 kg) of unclad UO_2 pellets to a fluid bed of alumina (32 kg) in the 6-in.-dia reactor and contacting the pellets at 350°C for 4 hr with gaseous reagents (N_2 or N_2 and HCl) containing small concentrations of oxygen. The off-gas from the fluid-bed reactor was filtered through an 11.5-in.-deep packed bed (14.7 kg) of 14 to 48 mesh alumina particles. It was observed that the presence of up to 2.5 v/o oxygen in the reactant gas mixture did not result in significant reaction of the UO_2 pellets. Less than 5% of the UO_2 charged to the fluid-bed reactor was converted to U_3O_8 fines. The packed-bed filter appeared to be highly efficient in retaining uranium fines, since the uranium loss by transport of U_3O_8 fines through the packed-bed filter was $<0.002\%$ of the UO_2 charge.

A decladding test was performed in which six 28-in.-long Zircaloy-2-fuel rods containing sintered UO_2 pellets were submerged in a fluidized bed of alumina particles and contacted with a gas mixture containing 60 v/o HCl, less than 0.04 v/o oxygen, and nitrogen for 4 hr at 400°C. The volatile zirconium tetrachloride produced by the reaction of the cladding with HCl was converted to solid oxide by steam in a separate fluid-bed reactor. The progress of the decladding reaction was satisfactorily monitored both by gamma-ray photographs of the fluid-bed section of the reactor and by continuous hydrogen analysis of the off-gas stream. The temperatures of the fuel rods, measured by skin thermocouples mechanically affixed at various heights to the cladding, were nearly identical to those of the fluidized bed throughout the run. There were no significant effects on the UO_2 pellets during the decladding step.

Development studies are being performed in a 2-in.-dia fluid-bed reactor to determine conditions for fluorinating UO_2-PuO_2 pellets containing fission products that would result in a minimum retention of uranium and plutonium on the fluid bed of alumina particles. Two runs were

completed in which 2-in.-deep beds of UO_2-PuO_2-fission product pellets were reacted using the following reaction sequence: (1) a two-zone oxidation-fluorination step (see Progress Report for January 1965, ANL-7003, pp. 58-59) at 450°C for 3 hr, (2) a single-zone fluorination step at 450°C for 2 hr with 7 v/o fluorine in nitrogen, and (3) a recycle-fluorination step with 90 v/o fluorine at 450°C for 1 hr, 500°C for 3 hr, and 550°C for 8 hr.

At the start of the recycle-fluorination step, the fluorine concentration was slowly increased from 7 to 70 v/o during a period of 45 min, and then increased at a more rapid rate to 90 v/o. This procedure was adopted to avoid the formation of agglomerates of bed material as a result of local temperature excursions in the bed, which might be produced by a high fluorine concentration at the onset of the recycle-fluorination step (see Progress Report for June 1965, ANL-7071, pp. 44-45). In one run the final bed material was entirely free of agglomerates or caked material; in the other run, only two small agglomerates were found.

Plutonium and uranium analyses from the final alumina bed from a run for which analytical results are available were 0.007 w/o and 0.003 w/o, respectively, representing a plutonium removal of 97.3% and a uranium removal of >99.9% for a single use of the alumina bed. These values are identical to those reported previously (see Progress Report for May 1965, ANL-7046, pp. 58-59) in which the duration of the entire fluorination cycle was 28 hr, in contrast to 17 hr in the present tests.

(iii) Engineering-scale Alpha Facility. A fluorinator for processing batches of UO_2-PuO_2 pellets to hexafluorides and a converter for transforming the mixed hexafluorides to a mixed particulate oxide form have been installed in an engineering-scale alpha facility. These units are undergoing shakedown tests with uranium materials under simulated alpha conditions, that is, the two gloveboxes that comprise the alpha facility are maintained at the design negative pressure (0.5 in. water), and all mechanical operations within the gloveboxes (charging, unloading, sampling) are carried out with gloves in place (see Progress Report for April 1965, ANL-7045, pp. 42-43). In a shakedown test, an 8.8-kg charge of UO_2 pellets was completely fluorinated to UF_6 in the fluorinator, and approximately one-half of the UF_6 product was processed to oxide in the converter reactor.

The fluorination of the UO_2 pellets was originally planned to be carried out using the two-zone oxidation-fluorination procedure (see Progress Report for January 1965, ANL-7003, pp. 58-59); however, processing difficulties occurred after 1 hr of operation when diluted fluorine was inadvertently admitted to the pellet zone through a side inlet, resulting in localized temperature excursions (to 800°C) and caking of the alumina bed material. The fluorination procedure was modified to

a direct fluorination scheme (both fluorine and oxygen admitted at the bottom of the reactor). This change allowed the run to be completed satisfactorily.

After about 60% of the UO_2 had been fluorinated, the system was put on off-gas recycle with 12 to 30 v/o fluorine in the reactant gas stream. The fluorination step was completed using 90 v/o fluorine.

Rates of production of uranium hexafluoride as high as 1.5 kg/hr were achieved during the recycle-fluorination period. An overall fluorine utilization efficiency of about 45% was achieved. The uranium concentration of both caked alumina material (~60 g) in the bed and the bulk alumina bed was 0.05 w/o, representing a uranium recovery of 99.97% of the UO_2 charged to the fluorinator. The UF_6-product collection system was highly efficient; over 99.8% of the UF_6 product was collected in the two refrigerated condensers and the sodium fluoride back-up trap.

In the fluid-bed converter reactor, a total of 5.5 kg of UF_6 was processed to UO_2 in 15 hr of operation at UF_6 flow rates of 10 and 18 g/min. The operating procedure involved alternating 30-min UF_6-steam-hydrogen feeding periods with 30-min periods in which only steam and hydrogen were fed to the reactor to remove residual fluoride from the UO_2 product. The UO_2 particle size in the bed was controlled effectively by in situ oxidation-reduction of the UO_2 particles.

2. General Chemistry and Chemical Engineering

a. Carbide-fuel Preparation. The carbide fuels show promise as fast reactor fuels capable of withstanding high burnup and having high thermal conductivity and high fertile or fissionable atom density. The importance of controlling the carbon-to-metal atom ratio in carbide fuels is well-known. An excess of carbon will cause carburizing and failure of cladding, whereas a deficiency of carbon will result in pockets of low-melting metal, which can also cause cladding failure. Efforts are being made to develop better methods for the preparation of carbide fuels.

Various methods for the preparation of uranium monocarbide have been studied. The liquid-metal technique has produced a powdered product with excellent pressing and sintering properties. In this process, carbon is added to a solution of uranium in zinc-magnesium at 800°C, uranium monocarbide is precipitated, and magnesium and zinc are removed by siphoning and distillation (see Progress Report for February 1964, ANL-6860, p. 80).

In another technique, uranium metal powder is contacted with a hydrogen-propane mixture in a fluidized bed at 500 to 700°C. Uranium

monocarbide has been prepared by this method on a 100-g scale in a 1-in.-dia fluid-bed reactor (see, for example, Progress Report for December 1964, ANL-6997, p. 45). The process variables (C:H ratio, temperature, gas flow rate, reaction time, and equipment design) have been studied. It was demonstrated that the carbon content of the carbide product could be controlled by the proper choices of C:H ratio and temperature, and that the fluidized-bed process shows promise as a method for the preparation of carbide fuels.

For large fast breeder reactors, the fuel would consist of mixtures of uranium and plutonium. A solid-solution fuel of (U-Pu)C would be desirable for heat transfer and particularly desirable from the standpoint of reactor safety (Doppler effect). Initial efforts were directed toward studying the feasibility of preparing such a solid solution by the reaction of UCl_3 and $PuCl_3$ with Mg_2C_3 in a molten salt mixture. In several preliminary experiments with UCl_3 alone, the product of the reaction was uranium monocarbide (UC). With $PuCl_3$ alone, the product was plutonium sesquicarbide (Pu_2C_3). In five experiments with mixtures of UCl_3 and $PuCl_3$, X-ray-diffraction analyses of the products indicated the presence of sesquicarbide phases in addition to the desired monocarbide phase. Work on this method of preparation was not pursued further (see Progress Report for October 1964, ANL-6965, p. 77).

Because of the success achieved in the preparation of uranium monocarbide by the fluidized-bed process, the feasibility of this technique for the preparation of (U-Pu)C solid solution is currently being examined. This method offers substantial potential savings in comparison to the technique which has thus far been given the most attention, namely, that of solid-solid reaction of uranium and plutonium dioxides with carbon. The main advantages of the fluidized-bed method are that it can be easily automated and can be controlled remotely. It is estimated that production rates as high as 10 kg/hr can be obtained from a single, critically safe, fluidized-bed reactor.

Prior to the preparation of (U-Pu)C in a fluidized bed, experiments are being performed utilizing a thermobalance to measure the extent of reaction of hydrided uranium-plutonium alloy with propane-hydrogen mixtures. The primary purpose of these experiments is to establish that a (U-Pu)C solid solution is formed by the reaction. Further aims are to establish that the use of the appropriate gas composition will limit the reaction to the formation of the monocarbide phase and to identify and evaluate the variables in the reaction.

In the thermobalance experiments, the weight change is recorded as a function of time. While the sample of uranium-plutonium hydride (prepared from a uranium-20% plutonium alloy) is suspended in a furnace from a balance pan, it is reacted with a flowing stream of propane and

hydrogen. In preliminary runs with pure propane, the weight gain was larger than that calculated for formation of (U-Pu)C, and the specimens contained free carbon. Subsequent experiments utilized hydrogen-to-carbon ratios for which the solid phase in equilibrium with the gas would be expected to be the monocarbide. The weight gains during the runs, the carbon analyses and X-ray lattice parameters of the products, and the monophasic structure of the pressed-and-sintered products indicated that the desired monocarbide phase was obtained.

Since the thermobalance experiments have indicated the feasibility of (U-Pu)C preparation by the use of propane-hydrogen gas mixtures, preparations are underway to test the fluidized-bed concept for this process. A 1.5-in.-dia fluidized-bed reactor is currently being installed in an alpha facility for this purpose. In addition, a larger fluidized-bed reactor system is being designed in which engineering data required for plant-scale production of (U-Pu)C can be obtained. It is anticipated that initially this equipment will be tested by preparing UC on a scale of 1 to 2 kg per batch. At a later date, it will be used to make (U-Pu)C.

3. Critical Constants of Alkali Metals

Studies to determine the critical constants of alkali metals have been continued (see Progress Report for November 1964, ANL-6977, pp. 70-71). Knowledge of the critical constants permits calculation of many thermodynamic and physical properties at temperatures between the boiling point and the critical point, a region for which such information is lacking. Thermodynamic properties of alkali metals are of particular interest because of their use as heat-exchange media in nuclear reactors.

The critical temperature and critical density of alkali metals were determined by a method which utilize radioactive isotopes of the alkali metals. The vapor and liquid densities of sodium, potassium, rubidium, and cesium were measured from room temperature to near the critical point by means of a radioactive counting technique (see ANL-6977, pp. 70-71).

The critical temperature and critical density were obtained by several methods of correlation. These included the rectilinear diameter plots of Cailletet and Mathias,[11] and correlations developed by Rowlinson[12] and by Kordes.[13] From the values of critical temperature and density so obtained, the generalized correlation of reduced density with reduced temperature shown in Figure 11 was prepared. This general correlation also appears to hold for lithium data based on reported

[11]Cailletet, L., and Mathias, E., Compt. Rend., 102, 1202 (1886).
[12]Rowlinson, J. S., Liquids and Liquid Mixtures, Academic Press, Inc., New York (1959), p. 92.
[13]Kordes, E., Z. Electrochem., 57, 731-738 (1953).

low-temperature (<1000°C) liquid densities.[14] The lithium data are also shown in Figure 12. Values of critical temperature and critical density based on the generalized correlation are listed below.

Element	Critical Temperature, °K	Critical Density g/cc
Cs	2057 ± 38	0.428 ± 0.013
Rb	2093 ± 35	0.346 ± 0.008
K	2223 ± 330	0.194 ± 0.038
Na	2573 ± 350	0.205 ± 0.042
Li	3223 ± 600	0.120 ± 0.033

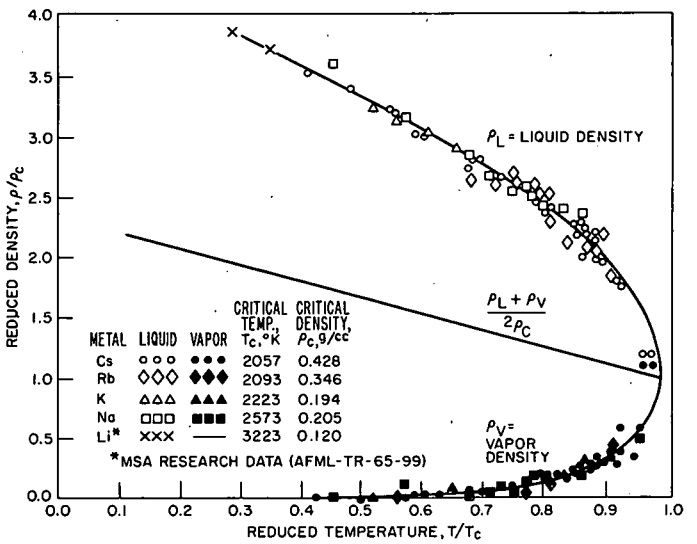

Figure 12
Generalized Correlation of Reduced Density with Reduced Temperature for Alkali Metals

4. Preparation of ^{24}Mg

The Chemical Engineering Division has been requested by the Physics Division (Argonne, Illinois) to prepare 100 g of ^{24}MgO. A reduction procedure based on a high-temperature (>1150°C) reaction of MgO and CaO and aluminum appears promising. When the reduction is conducted in vacuum, the metallic magnesium product is volatilized:

$$3MgO + CaO + 2Al \rightarrow 3Mg + Ca(AlO_2)_2.$$

Magnesium yields of 100% have been reported when pelletized mixtures containing stoichiometric amounts of MgO and CaO and approximately twice the amount of aluminum necessary for complete MgO reduction were heated in vacuum at temperatures from 1150 to 1225°C.[15] During the past month, laboratory equipment has been installed to carry out the testing of the above procedure.

[14]Tepper, F., Zelenak, J., Roehlich, R., and May, V., AFML-TR-65-99 (May 1965).
[15]Improvements Relating to the Production of Magnesium, British Patent No. 569,744 (1945).

G. Sodium Coolant Chemistry

1. Control of Sodium Oxide Impurities

a. United Nuclear Electrochemical Oxygen Meter Field Test. The sodium oxide-impurity-control loop was modified for field testing two United Nuclear Electrochemical oxygen cells in series in a bypass loop. Housings for the ceramic probes were welded in place, and dummy stainless steel probes, displacing the same volume of sodium as the ceramic probes, were installed for preliminary testing of flow and temperature control.

The dummy probe in housing #1 was replaced by the ceramic probe and the sodium system brought up to 600°F, the recommended operating temperature. Cell differential voltage readings taken at about hourly intervals ranged from 1.073 to 1.064. Flow of sodium through the cell was calculated to be 0.79 gpm.

While the bypass line was frozen, the sodium in housing #2 was heated to about 250°F and an attempt was made to replace the dummy probe with a ceramic cell. An estimated insertion rate of about 2 min was apparently too rapid, causing a thermal shock which shattered the ceramic tube. The broken pieces were too small to be removed with tweezers. After freezing the sodium, the housing was cut out, emptied, cleaned, rewelded in place, and a dummy probe inserted for lack of another ceramic cell.

Since the cell in housing #1 was still in working order, another run was made with sodium at 600°F. The voltage reading of the cell was 1.070 V. About one hour later, the low-level alarm in the surge tank became activated (due probably to leakage of sodium through a valve back into the 5000-gal tank), shutting off the power to the pump and stopping flow through the loop. When sufficient sodium was drawn into the loop by a vacuum pump on the surge tank to permit the pump to operate, about 15 to 20 min had elapsed. At this time, the voltage of the oxygen cell was found to be about 0.001 V, suggesting that the cell was shorted, probably due to a crack in the ceramic. Removal of the cell and visual examination confirmed the presence of a crack, opened about 1/32 in. over part of its length. It is believed that a thermal shock occurred as the result of this accidental flow stoppage. Plans to prevent a recurrence are under study.

H. Plutonium Recycle Reactors

1. Reactor Vessel Cladding

a. Safety Analysis. An analysis has been made of the possible effects on safety of the cracked cladding of the reactor vessel. This

analysis demonstrates that safety of the vessel is not compromised by failures of the cladding inasmuch as the strength of the cladding was not previously utilized in the calculations of the strength of the vessel. The strength of the vessel still more than meets the safety requirements of the ASME Code for "Power Boilers," which was the original design criterion. A surveillance program to study both the mechanism of propagation of the cladding crack and the corrosion of the limited areas of bare vessel wall is being carried out.

A report summarizing the results of the nondestructive examination of the vessel, and repairs of primary system piping and auxiliary equipment is in preparation. On completion of repairs, these components will meet the safety requirements of the ASME "Unfired Pressure Vessel" and ASA B31.1 "Power Piping" Codes for continued service at 600 psig steam pressure.

b. Investigation of Causes of Cracking of the Clad. Metallographic examinations of the three clad SA 212B plate samples were completed (see Progress Report for June 1965, ANL-7071, p. 49). Photomicrographic studies of the cladding revealed three unrelated cracking mechanisms.

(i) Through-cracking of SS 304 Cladding. Through-cracking of the cladding with propagation from the exterior SS surface to the carbon steel interface and simultaneous propagations from both surfaces were observed and documented. Although there is no direct evidence for the mechanism, the ruptures are believed to be biaxial thermal-stress ruptures generated in the spot-welding process.

The model for the mechanism of cladding cracking comes from a consideration of the spot-welding process. In the process, linear rows of "thumb-print" nuggets were formed one at a time sequentially at short time intervals. Neighboring rows were formed on the return portion of the machine welding cycle. In consequence, a thermal gradient was maintained between linear nugget neighbors and neighboring rows throughout the cladding operation. The photomicrographic evidence for the rapid cooling of the melted cladding is the fine-grained transformed structure of the SS 304 kernel and the underlying transformed structure of the carbon steel plate at the bond interface. Since the thermal conductivity of the carbon steel plate is greater than the overall heat transfer coefficient to coolant water, the bond region was cooler and stronger than the heated and unmelted cladding above the kernel. Further cooling increased thermal stresses until rupture occurred. Minor through-cracking of the flat clad plates during the fabrication of the vessel was detected and repaired by welding.

(ii) Lamellar Cracking of SS 304 Cladding. Lamellar cracking of the cladding was observed in the formed vessel shell section and in the clad test plate rolled to the 42-in. radius of the EBWR vessel. Although there is no direct metallographic evidence for shear-type failures, the ruptures are believed to be associated with the "normalizing" heat treatment of the SA 212B plate, which consists of heating the carbon steel plate to the austenitizing temperature of the steel (1600/1650°F) followed by cooling in still air. The heat treatment yields a shell steel with a uniform structure.

At the normalizing temperature, both the carbon and SS 304 steels are plastic, and since holding time at temperature is long (one hour per inch of thickness), residual stresses are relaxed. In the cooling process, both steels contract but not uniformly; the coefficient of expansion (contraction) is greater for the SS 304 than for the carbon steel. Tensile stresses are induced in SS 304 while the base carbon steel is stressed in compression; stress intensities are inversely proportional to the thicknesses of the two members joined.

Since the members are mutually loaded by the spot welds, the tensile cladding forces are transmitted to the much thicker backing plate by bending moments. The stiffness of the beam sections are proportional to thickness squared.

A simplified analysis of a composite beam consisting of a 0.109-in.-thick SS 304 cladding attached to the $2\frac{7}{16}$-in. carbon steel backing shows that the spot-welded-on cladding will rupture, in tension, when cooled from the normalizing temperature.

(iii) Radial Cracking from Weld Nugget. Micrographs of the longitudinal and transverse sections show that the kernel of the nugget is an oblate ellipsoid. This kernel was melted by the passage of welding current, and its cross section is substantially larger than the bond area. The kernel is surrounded by unmelted wrought SS 304 and the carbon steel base plate. This is a contained hydraulic system which was ruptured by the molten SS 304 core. The failure of a membrane by hydrostatic pressure is radial with cracks normal to the surface, substantially as observed. Also observed were extrusions of molten SS 304 into the microvoids at the SA 212B boundary.

2. Reactor System Piping

Repairs of substandard welds in the primary piping system between the reactor face and the first fluid-flow control valve inside the containment shell were continued. Radiographic examinations of repaired welds required an additional nominal amount of repair work.

The Materials Testing Laboratory completed the radiographic inspection of 39-in. steam-supply line welds to the two blocking valves at the primary reboilers. Part of this primary 600-psi-steam line is inside the containment shell, and the rest is in the tunnel and reboiler building outside the containment shell. Inspection of the 8-in. steam line was included to establish its integrity following the severe service of the 100-MW operations of EBWR. At reactor powers above 70 MW, this piping was strongly shock excited by entrained slugs of water.

III. ADVANCED SYSTEMS RESEARCH AND DEVELOPMENT

A. Argonne Advanced Research Reactor (AARR)

1. Critical Experiments

Measurements were continued with aluminum beam-tube mock-ups in the reflector, using the 810-fuel-foil system (see Progress Report for June 1965, ANL-7071, pp. 51-56). The locations of these beam tubes are shown in Figure 13.

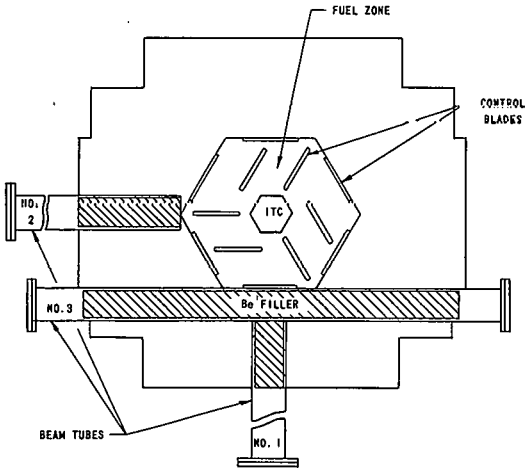

Figure 13. Locations of Beam Tubes and Beryllium Fillers

As reported earlier (ANL-7071, p. 55), the installation of air filled beam tubes reduced reactivity by 1.2%. Insertion of beryllium filler plugs in the beam tubes (see Figure 13, shaded areas of the beam tubes) restored approximately 81% of the original beryllium volume; the total reactivity worth of these plugs was measured as +1.0%. The remaining net reactivity loss therefore is attributable to the composite of: (a) the aluminum beam-tube walls; (b) some void in the beam tube due to incomplete filling with beryllium plugs; and (c) the removal of some of the water reflector beyond the beryllium. Direct measurements will be made of the reactivity worth of aluminum in the reflector.

The reactivity effect of removing the beryllium fillers of each individual beam tube was measured. For beam tube No. 1, removal of beryllium corresponded to -0.08%; for No. 2, -0.2%; and, for No. 3, -0.6%. Note that the sum of the individual worths is somewhat smaller, in absolute magnitude, than the worth of voiding all 3 beam tubes.

Activation traverses have been made with manganese foils for two cases. For Case I, the beam tubes were voided; for Case II, beryllium filler plugs were inserted. The locations of the manganese foils for these measurements are shown in Figures 14 and 15, respectively. The traverses for Case I are shown in Figure 16; and traverses for Case II are shown in Figures 17 and 18. Figures 16 and 17 may be compared with traverses made earlier in the system without beam tubes (see Progress Report for May 1965, ANL-7046, p. 72, Figure 19). The relative activity of the bare manganese foils is reduced considerably when the beam tube is voided; it is reduced, but only slightly, when beryllium filler plugs are inserted.

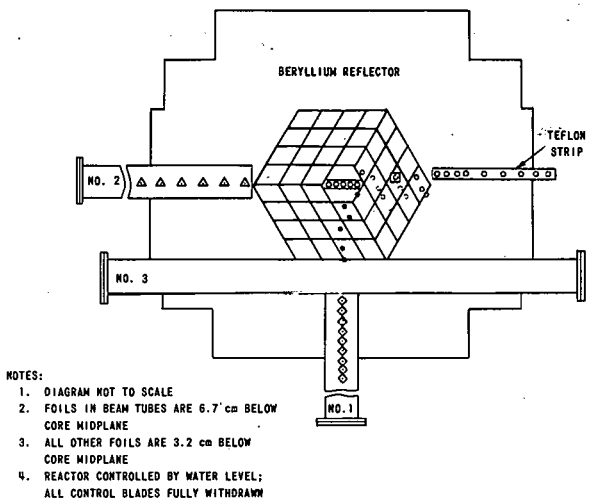

Figure 14. Cross Section View of Beam Tubes; Foil Locations (Beam Tubes Voided)

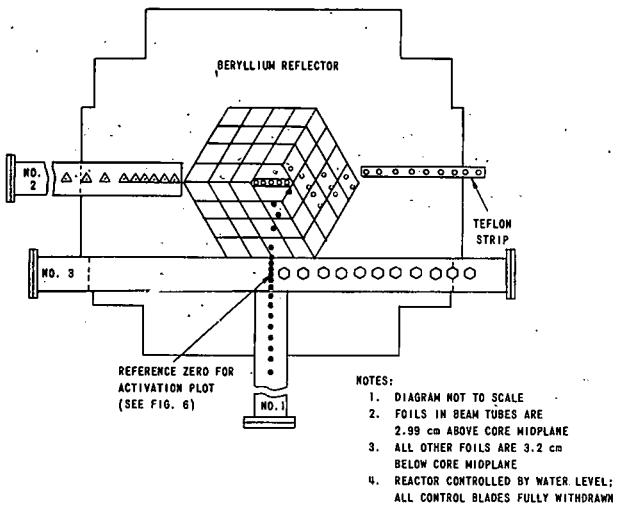

Figure 15. Cross Section View of Beam Tubes; Foil Locations (Beam Tubes Filled with Beryllium)

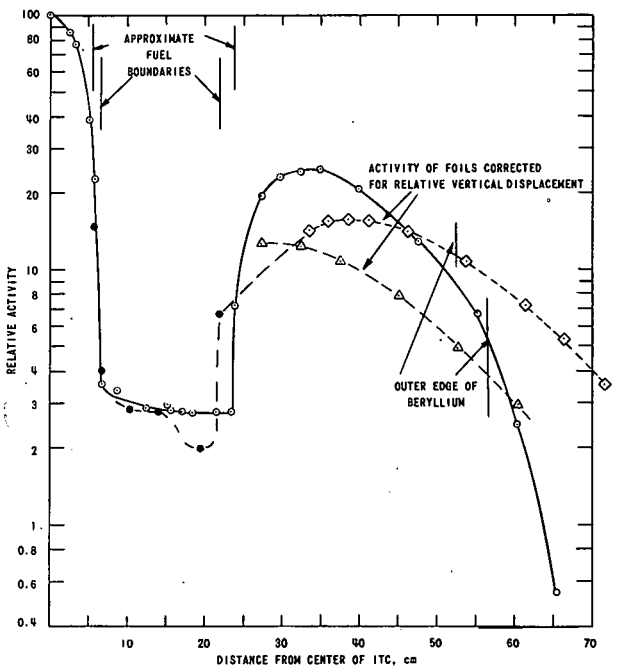

Figure 16

Radial Traverses with Bare Manganese Foils in the 810-fuel-foil System with Voided Beam Tubes

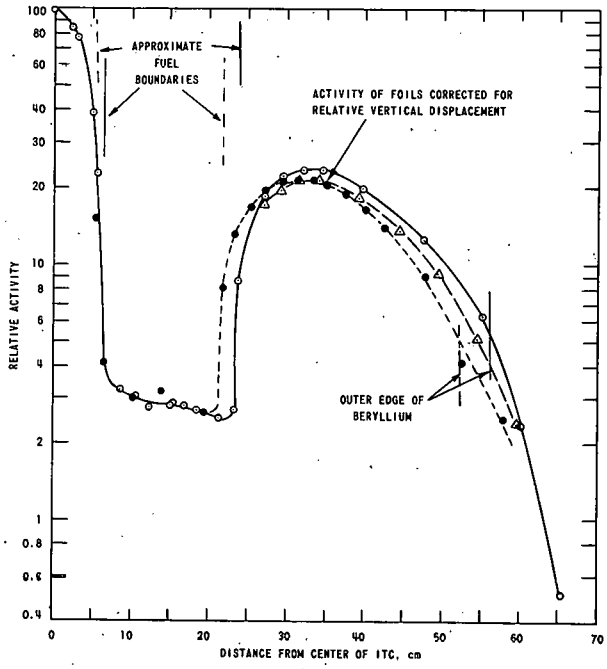

Figure 17
Radial Traverseses with Bare Manganese Foils in the 810-fuel-foil System with Beryllium Filler Plugs in the Beam Tubes

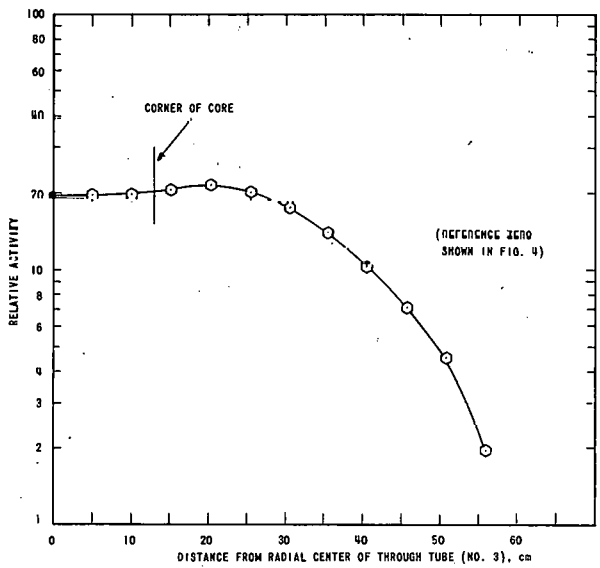

Figure 18
Traverse with Bare Manganese Foils in the Through Tube (810-fuel-foil System; Beryllium Filler Plugs in the Beam Tubes)

Figure 18 shows a plot of the relative activity of bare manganese foils in the through tube (No. 3). There is little variation along the adjacent core face, with a slight peaking occurring approximately 3 in. beyond the corner of the core.

Additional measurements of reactivity and detector-activity distributions are planned with beam tubes in the reflector.

The U^{235} (fission) cadmium ratio has been measured in the core of the 810-fuel-foil loading. At the position indicated by a hollow square (□) in Figure 14, the cadmium ratio was 1.65 ± 0.05.

Argonne has been notified that the fuel-foil supplier will make no further attempt to produce the thinnest foils on order, namely, the 0.00055-in.-thick uranium foils. The supplier asserts that they are unable to fabricate these foils with the equipment available. The remaining fuel foils, including the supplemental order of 120 0.0044-in.-thick foils, are being produced at a fairly steady rate.

2. Hazards Analysis

The hypothetical case of a massive contamination of the sealed reactor containment building of AARR, an accompanying rise in building pressure, and ground-level leakage of contaminated air has been studied very conservatively for purposes of the Preliminary Safety Analysis Report (PSAR). In particular, the effect of turbulence in the vicinity of ground level on the leeward side of the building is to reduce the concentration of fission products at the axial centerline of the plume which would develop from the ground-level source. This effect has not been included in earlier AARR studies.

According to Gifford's analysis,[16] the result of such turbulence is to reduce certain dose rates from such a plume by

$$\frac{100\ cA}{\pi\sigma_y(x)\sigma_z(x) + cA}\%.$$

The terms $\sigma_y(x)$ and $\sigma_z(x)$ are dispersion functions evaluated at a distance x (in meters) from a single, ground-level point source. The constant c is the estimated size of the pressure wake in relation to A, the cross-sectional area (in square meters) of the containment building, measured normal to the wind velocity vector. The application of this formula is limited to those dose rates which depend strongly upon the concentration of fission products at the axial centerline of the plume, for example, the inhalation-dose rate.

For the reactor containment building of AARR, as presently conceived, $A = 900\ m^2$. At $x = 100$ m, $\pi\sigma_y(x)\sigma_z(x) = 29\ m^2$, based on "moderately stable" atmospheric conditions.[17] For a conservative value, $c = 0.1$, there is a 75% reduction in inhalation-dose rate at 100 m. Much larger values of $c (c > 0.5)$ have been suggested.[16] For $c = 0.5$, the inhalation-dose rate at 100 m would be reduced by 94% according to this analysis.

[16] Gifford, Jr., F. A., Atmospheric Dispersion Calculations Using the Generalized Gaussian Plume Model, Nuclear Safety 2(2), 56-59 (Dec 1960).

[17] Gifford, Jr., F. A., Use of Routine Meteorological Observations for Estimating Atmospheric Dispersion, Nuclear Safety 2(4), 47-51 (June 1961).

3. Heat Transfer

a. Analytical Studies. The study of thermal transients occurring at high power levels was continued (see Progress Report for June 1965, ANL-7071, pp. 56-57). A preliminary investigation has been made of the CHICK-IN[18] computer program, with particular emphasis on its suitability for AARR hot-channel transient analysis. The program, currently in test with the CDC-3600, was developed by the Bettis Laboratory for analysis of rapid transients in water-moderated reactors.

It was concluded that although deficient in some respects, the CHICK-IN program will be of value in AARR hot-channel transient analysis for the following reasons:

(i) The program can predict fuel-plate temperatures for reactivity-induced transients while taking into account conditions beyond departure from nucleate boiling and/or flow stoppage in channels.

(ii) It will provide local values of fluid pressure, enthalpy, flow rate, plate temperature, and heat flux during transients, which will be useful in evaluating assumptions regarding the existing model as well as lend guidance in the construction of improved future models.

b. Experimental Program. Test Section IV, with a flow channel 0.040 x 1.25 x 18 in. long, has been installed in the Steady State Loop. The analysis of data from test Section III (see Progress Report for April 1965, ANL-7045, p. 54) is in progress.

Experiments in the Transient Loop to determine the feasibility of using the 1500-kW DC power supply for transient tests are still in progress. The study of response time to achieve peak power has been enhanced by the use of an auxiliary round-tube test section cooled by tap water under normal line pressure. Response time has been further reduced from 46 msec (see Progress Report for June 1965, ANL-7071, p. 57) to 40 msec; however, the ratio of peak power to initial power was less than that achievable with the longer response times.

Changes of the power-supply control circuit will allow use of the round tube. Another circuit is being designed to control the ratio of, and time between, initial and peak power.

Development work on the AARR Shutdown Cooling Test sections has been completed. The 0.040 x 1.0-in. rectangular channels were formed

[18]Redfield, J. A., CHICK-IN--a FORTRAN Program for Intermediate and Fast Transients in a Water Moderated Reactor, WAPD-TM-479 (Jan 1965).

from 0.75-in.-OD seamless 304 SS tubing, annealed once before final forming and dimensioning. The test sections are now ready for attachment of power terminals and inlet and outlet transition pieces.

4. Hydraulic Tests

A device to measure fuel-plate distortion or vibration during hydraulic testing is being developed. Two restrictions of considerable import have been placed on the design: (a) the device must not appreciably affect the flow pattern over the fuel plates, and (b) it must not impose any physical loading on the fuel plates.

The developmental effort is divided into two studies: one for low temperature (below 200°F) and another for high temperature (below 500°F). Currently available instrumentation appears to be suitable for the low-temperature application only; as a result, an electronic, capacitance-type device has been built and is being tested for use at high temperatures.

5. Primary System and Components

Oak Ridge National Laboratory will make a series of corrosion tests to investigate problems which may arise in the AARR primary system. Deposition, primarily of anodic material onto the stainless steel fuel cladding, and general corrosion rates will be studied in loops simulating metal-surface-area to water-volume ratio in the multimetal AARR system. There will also be a separate investigation of beryllium and beryllium-aluminum corrosion.

Two small specimens of beryllium with a combined surface area of 12.5 cm^2 have been exposed to deionized water at 200°F flowing at a velocity of 44 fps. The total volume of the loop system is 27.6 liters. Weight losses were determined after 97 hr of exposure and again after an additional exposure of 381 hr, for a total time of 478 hr. The results are:

	Specimen No. 1		Specimen No. 2	
Total time, hr	Weight loss, mg/cm^2	Corrosion rate, mg/yr	Weight loss, mg/cm^2	Corrosion rate, mg/yr
97	0.19	3.6	0.24	4.6
478	0.70	2.7	0.80	3.1

The specimens developed a very thin tarnish film and one small pit, no more than a few mils thick, on an edge of one of the pieces. The specimens will be exposed for an additional 500 hr.

Most of the equipment for evaluating the thermal effect of the corrosion of the aluminum beam tubes has been assembled. An electrically heated aluminum specimen (6061-T6), mounted in a bypass line of a second loop, will be cooled by water flowing at 10 fps past the specimen. The heat flux across the walls of the specimen will be adjusted to obtain a specimen surface temperature of 260°F with a bulk water temperature at 150°F. Calculations indicate that a heat flux of about 175,000 Btu/hr-ft^2 will be required to achieve the desired surface temperature.

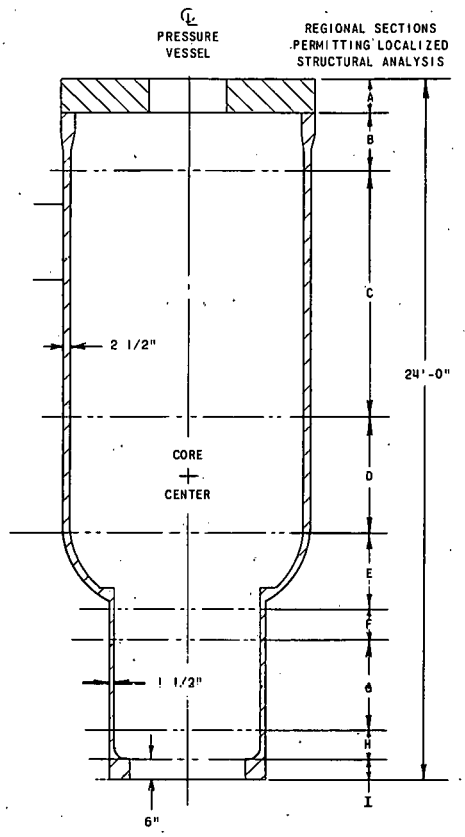

Figure 19. Model AARR Pressure Vessel for Stress Analysis #1

6. Stress Studies of the Reactor Vessel

The preliminary stress analysis for the AARR vessel (see Figure 19) has been completed. In the analysis, the vessel was divided into more simple structural shapes or regions such as rings, short transition cylinders, long cylinders and tapered curved beams for which stress and deformation equations are well known. These were separated at hypothetical interface planes, and deformation of each member under the applied load was calculated, assuming the member to be independent of adjacent members. The calculated deformations between adjacent members were, of course, unequal, since members of differing geometries behave differently under the load. The members were then hypothetically reassembled, and the assumption was made that under load, discontinuity moments and shear forces were generated to counteract the differences in the independent-member deformations, to maintain vessel continuity.

The magnitudes of the unknown discontinuity moments and shear forces were found from the requirement that the deflection and rotation caused by these moments, shear forces, and internal pressure must be continuous across each interface. Once the discontinuity moments and shear forces were determined, the stresses in each member of the vessel were calculated.

The stresses in the various regions of the vessel caused by mechanical load and by differential thermal expansion are tabulated in Table XII. Apparently a large proportion of the stress in the vessel is caused by differential thermal expansion. This is to be expected because of the high flux of the reactor core and the consequent high rate of heat generation in the vessel wall. However, the low thermal conductivity and

the large coefficient of thermal expansion of the stainless steel aggravate the situation. If carbon steel were used, for example, the critical stress in region C could be reduced from 39,855 psi as listed in Table XII, to 24,384 psi.

Table XII. Stress Intensities (psi) in AARR Pressure Vessel

Region	Primary P_m General Membrane	Primary P_L Local Membrane	P_b Bending	Primary + Secondary P_m(or P_L) + P_b + Q	Remarks
A			25,500	26,802	
B		19,350		44,350	
C	16,570			39,855	
D		17,519		42,519	Assuming no nozzles
E		17,660		43,412	
F		25,981		43,191	
G	14,750			30,402	
H		38,896		56,106	P_L can be reduced by increasing fillet radius
I			13,100	16,316	

Based on the preliminary stress analysis, a design change is presently being contemplated. A second concept under investigation is shown in Figure 20, in which the lower section has been enlarged to eliminate a high stress area caused by the coolant nozzle intersection with the reduced vessel section. The new concept shows the vessel as having an 8-ft dia throughout and increased from 24 to 26 ft in length.

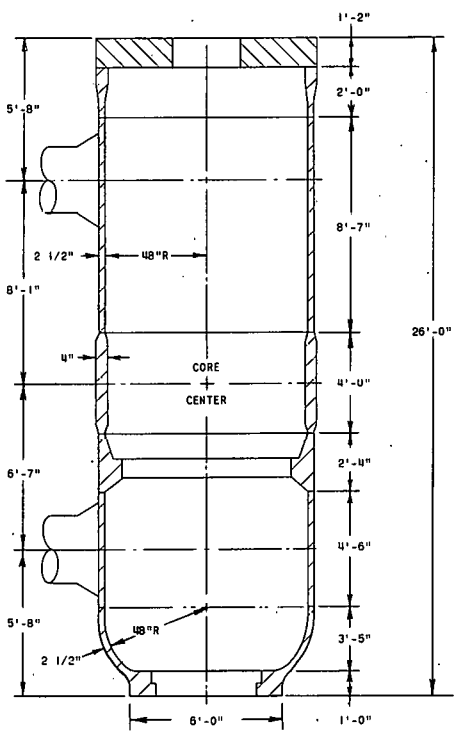

Figure 20
Model AARR Pressure Vessel for Stress Analysis #2

IV. NUCLEAR SAFETY

A. Reactor Kinetics

Two key characteristics of core designs for large fast power reactors are: 1) the large amount of fuel, and 2) the short prompt-neutron lifetime. Because, typically, there are several critical masses of fuel present, it is possible to hypothesize a class of "meltdown" accidents in which some abnormal conditions cause a minor accident that, in turn, produces rapid motion of core material into a more reactive configuration and finally results in a release of nuclear energy. In order to analyze the course of such accidents or, indeed, determine whether they can occur, it is necessary to obtain information on mechanisms of fuel failure, coolant movement, fuel movement, and interplay of the various phenomena involved in meltdown incidents. Because of the complexity of the problem, a program of in-pile experiments is underway in the TREAT reactor to study meltdown phenomena experimentally. In addition, associated effort is underway to develop theoretical tools for analyzing results, special instrumentation for the experiments, out-of-pile experiments to obtain basic data necessary to the understanding of the relevant phenomena, and theoretical extrapolations of basic data. Periodic accident studies are also necessary to check the significance of the results to power reactor designs.

1. Fast-neutron Hodoscope

The 50-channel hodoscope for monitoring fuel motion during meltdown experiments in TREAT by detecting prompt neutrons released by fissions in the sample (see Progress Report for January 1965, ANL-7003, p. 39) has been completed and sent to the TREAT reactor for testing under actual experimental conditions. This device is designed to provide time resolution of the order of 1 msec and space resolution of 0.32 cm horizontal by 1.3 cm vertical, with adequate signal-to-background ratio. The steel collimator contains 320 tapered holes machined at the proper angles for focusing on the test sample. The central 50 holes cover an area of about 5 cm wide by 30 cm high at the sample position in TREAT. The remaining holes can be used to vary sample coverage and are designed to permit eventual expansion to a system capable of observing large clusters in the large TREAT meltdown loop.

Three transparent meltdown capsules, each containing one 9% enriched EBR-II pin were shipped to the test reactor for neutron camera checkout. In addition, a transparent slot liner, modified by removal of the graphite from the end, was shipped for use with the transparent capsules. With this equipment it is possible to run a meltdown test using both optical and prompt-neutron detection systems for comparison, without the added background produced in the neutron system by the standard end graphite piece of the slot liner.

An integral sodium loop, containing one 6% enriched EBR-II pin surrounded by empty stainless steel EBR-II pin cladding tubes is also at TREAT, to be run in conjunction with the camera tests.

2. Effect of a Standard Approximation in Calculation of Fuel-temperature Distributions

It was pointed out (see Progress Report for April 1965, ANL-7045, p. 66) that neglect of the $(\partial k/\partial T)(\partial T/\partial r)^2$ term in the heat transfer equation for cylindrical geometry:

$$\frac{\partial T}{\partial \tau} = \frac{k}{\rho c_p}\left(\frac{\partial^2 T}{\partial r^2} + \frac{1}{r}\frac{\partial T}{\partial r}\right) + \frac{1}{\rho c_p}\frac{\partial k}{\partial T}\left(\frac{\partial T}{\partial r}\right)^2 + \frac{q}{\rho c_p}, \qquad (1)$$

where T is temperature, τ time, k thermal conductivity, ρc_p volumetric heat capacity, r radius, and q volumetric heat generation, can cause appreciable errors in some cases. In particular, when large thermal gradients and large changes in k as a function of temperature occur (as in the case of uranium oxide or uranium-plutonium mixed oxide) the term is significant. Equation (1) is often used in machine calculations of transient temperatures by assuming that k is essentially constant over the volume associated with each mesh point, resulting in the form

$$\frac{\partial T}{\partial \tau} = \frac{k}{\rho c_p}\left(\frac{\partial^2 T}{\partial r^2} + \frac{1}{r}\frac{\partial T}{\partial r}\right) + \frac{q}{\rho c_p}. \qquad (2)$$

which is used as the basis for the finite-difference equations put in the machine code.

If the transformation

$$d\theta = k\,dt \qquad (3)$$

is made, then Eq. (1) may be integrated to yield, for steady state,

$$\int_{T_2}^{T_2} k\,dt = \frac{qR^2}{4}, \qquad (4)$$

where T_1 is surface temperature, T_2 is central temperature, and R is outer radius.

A reasonable fit to experimental thermal-conductivity data for UO_2 reported by Kingery,[19] Reiswig,[20] and Hedge and Fieldhouse[21] is given by

[19]Kingery, W. D., et al., NYO-3647 (1953).
[20]Reisig, R. D., J. Am. Ceram. Soc., 36, 48 (1961).
[21]Hedge, J. C. and Fieldhouse, J. B., AECU-3381 (1956).

$$k = \frac{35}{T + 300} \text{ (in W/cm-°C)} \tag{5}$$

where T is given in degrees centigrade.

By means of Equations (4) and (5), a constant q was selected, together with an outer radius R of 0.200 cm, such that T_1 and T_2 would fall in the range of interest for a high-power-density UO_2 fuel rod. The value of T_2 was set at 2250°C (somewhat above the highest temperature-data point of Reiswig). Then, using an existing differential equation subroutine for the CDC 160A,[22] the problem was run with Equation (2) in the form for the steady-state case:

$$\frac{d^2t}{dr^2} + \frac{1}{r}\frac{dT}{dr} = \frac{T + 300}{35} q. \tag{6}$$

Equation (6) may be considered to be the limiting case of the ARGUS code, for an infinite number of mesh points, at each of which k(T) is reevaluated.

Figure 21 shows the radial temperature as a function of r/R from the exact calculation of the Equation (4) type, together with the limiting case of the ARGUS code given by Equation (6). Although the temperature difference at R is only 191°C, this corresponds to a difference in q, as calculated correctly by means of either Equation (1) or Equation (4), of 22%. If the calculations are normalized to the same T_1, the difference in values of T_2 is much higher: this case is also shown in Figure 21.

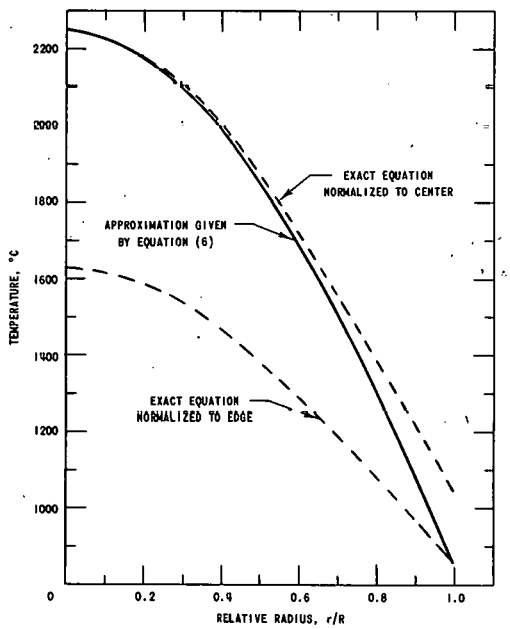

Figure 21

Radial Temperature Distribution of UO_2 Rod Based Upon Equations (4) (Dotted Curves) and (6) (Solid Curves)

[22] Lukehart, P. M., Comm. A.C.M. 6, 737 (1963).

One interesting feature of this problem is its independence of R. Equation (4) indicates that, if T_2 is fixed, T_1 remains constant as long as the product qR is maintained constant, and the curve of T(r/R) is unchanged. However, T(r/R) as calculated from Equation (6) also remains unchanged under the same conditions. Thus the discrepancy illustrated in Figure 21 is independent of R.

More detailed calculations on transient effects are underway.

3. Thermal Stresses

Thermal stresses of a cylindrical fuel pin made of U-15 w/o Pu-10 w/o Ti were calculated for temperature distributions typical of TREAT excursions. The mechanical properties of this material are strongly temperature dependent and are available in the form of experimentally determined curves. A graphical method was devised for calculating the radial distribution of the axial normal stress caused by a radially varying temperature field. This stress distribution was found by graphically evaluating

$$\sigma(r) = E[T(r)]\{e_A - e_T[T(r)]\},$$

with

$$e_A = \frac{2}{R^2 E_A}\int_0^R r\, E[T(r)]\, e_T[T(r)]\, dr;$$

$$E_A = \frac{2}{R^2}\int_0^R r\, E[T(r)]\, dr.$$

In the above R is the outer radius of the rod, T(r) is the prescribed temperature distribution, E is the Young's modulus, E_A is the average value of E for the cross section, e_T is the thermal strain in a uniformly heated test specimen at temperature T, and e_A is the average strain across the cross section; $e_T(T)$ and E(T) are known from plots of experimental data. For parabolic temperature distributions which varied between (a) 800°C at the centerline and 650°C at the surface, and (b) 850°C at the centerline and 750°C at the surface, it was found that $\sigma(r)$ varied between (a) $\sigma(0) = -15$ kg/mm^2 and $\sigma(R) = 10$ kg/mm^2, and (b) $\sigma(0) = 35$ kg/mm and $\sigma(R) = 16$ kg/mm^2. These stress levels are higher than the ultimate strength of the material at these temperatures, so cracking and failure would be expected.

B. TREAT

1. Operations

Two preirradiated uranium oxide samples were irradiated for ORNL to obtain data about fission product release.

A sample of prototype SEFOR fuel was subjected to eleven transient irradiations for the General Electric Company.

The reactor was reloaded for testing of the fast neutron hodoscope (see Section IV.A.1) for detecting fuel movement during meltdown experiments. Checkout of the electronics for the hodoscope is progressing satisfactorily, and initial testing using neutrons from a test pin in the reactor should start within a few days.

2. Large TREAT Loop

The major portion of the large test section is about 90% complete. Major problems were encountered in welding of Conoseal flange sections to the test section because one of the flanges was damaged in the initial installation; a new flange was purchased.

The vendor of the bellows plates for the surge suppressor portion of the test section reports these parts have been successfully formed and welded, and the assembled convolutions have passed the required tests. The delivery of the pressure-vessel end-caps which will house the bellows has been delayed, which will consequently delay the delivery of the surge suppressor.

The electrical portion of the leak detector has been assembled and is being checked. Grids will be installed as loop construction nears the final stages. Replacement bellows for the loop have been received from the vendor and are being inspected. In addition, delivery of the bellows which are to be used in the horizontal pipe sections at the top of the reactor will be delayed.

The transient-induced perturbations of sodium flow in the Large TREAT Loop were investigated theoretically by conventional force-balance techniques; the equations of motion were integrated numerically. This analysis was based on an instantaneous pressure rise in the test subassembly and a piston-like behavior of sodium entering the surge suppressor. The results (see Table XIII) indicate that the maximum upward displacement of sodium in the test section will not require a full bellows travel; thus, impact of the bellows upper plate and sodium against the top of the surge suppressor should not occur.

The peak pressures reached during Large TREAT Loop energy inputs of 6,000 and 10,000 Btu have been determined. The values agree closely with the peak pressure calculated previously.

Table XIII. Maximum Flow Perturbations

Condition Max Transient Pressure and Pre-transient Flow Rate	Max Velocity,(a) fps	Displacement at Max Velocity, ft	Max Displacement,(a) ft
250 psi			
40 gpm	26.01 (85)	1.64	2.46 (128)
80 gpm	27.44 (84)	1.72	2.49 (123)
160 gpm	30.39 (83)	1.92	2.56 (115)
500 psi			
40 gpm	42.73 (67)	2.03	2.85 (98)
80 gpm	43.98 (65)	2.03	2.88 (96)
160 gpm	46.56 (61)	2.03	2.94 (92)
750 psi			
40 gpm	54.79 (55)	2.09	3.14 (85)
80 gpm	55.96 (53)	2.06	3.17 (84)
160 gpm	58.40 (51)	2.09	3.23 (81)
1000 psi			
40 gpm	64.74 (48)	2.14	3.38 (77)
80 gpm	65.91 (47)	2.14	3.40 (76)
160 gpm	68.29 (45)	2.13	3.45 (74)

(a) The number in parentheses is the time, in milliseconds, at which the value is reached.

C. Chemical and Associated Energy-transfer Problems in Reactor Safety

1. Metal-water Reactions

a. High-temperature, High-pressure Furnace. Experiments designed to study the reactions of fuel cladding under conditions simulating the environment in a water-cooled power reactor following a loss-of-coolant accident have continued. The studies are carried out in a furnace which is designed for a maximum pressure of 1000 psig and sample temperatures as high as 1700°C (see Progress Report for November 1964, ANL-6977, p. 82). The furnace consists of two zones: an internal steam-filled zone that is surrounded by an alumina tube, and an external zone that is argon-filled. The argon-filled zone contains molybdenum heater windings and insulation. The pressures in the two zones are automatically matched to avoid stresses on the alumina tube. Water is introduced into the lower part of the steam zone by a positive-displacement pump and is converted to steam. At the start of an experiment, the sample is elevated from a

moderate-temperature section, where reaction with steam is negligible, into the high-temperature section. Some unreacted steam and the hydrogen produced by the metal-steam reaction are continuously removed from the upper part of the steam zone (high-temperature section) through an outlet valve. The extent and the rate of metal-steam reaction are determined by monitoring continuously the amount of hydrogen collected. Upon completion of the experiment, the sample is lowered to its initial position.

A sample (8 in. long by 0.4-in. OD) consists of a number of high-density UO_2 pellets clad with either Type 304 stainless steel or Zircaloy-2 tubing having a 27-mil wall thickness. The top and bottom of the tube are closed with 3/16-in.-thick welded plugs. The 2.5-mil radial gap between the UO_2 and the cladding is filled with helium at a pressure of 20 psia. A sample is raised into the high-temperature section of the furnace at the rate of 1 in./min, thus requiring a total of 8 min for complete insertion.

b. Reaction of Stainless Steel-clad Fuel Elements with Steam. A preliminary experiment with a Type 304 stainless steel-clad fuel element was described in the Progress Report for November 1964, ANL-6977, p. 83. In that experiment, which utilized a steam flow rate of about 1 ml/min of water, the fuel element remained in the hottest part of the furnace for 180 min. The upper two-thirds (hottest portion) of the cladding appeared to be reacted completely, most of the reaction occurring in the first 90 min. It was apparent from these results that the reaction rate was limited by the low flow rate of steam past the sample.

Experiments were performed to examine the effect of steam flow rate on the reaction rate. In the first set of experiments, the steam pressure was maintained at 1 atm and the flow rate was increased to 10 ml/min of water (85 liters/min of steam) with a nominal linear velocity of 1.5 ft/sec. The residence time of the fuel element in the hottest part of the furnace was greatly reduced. The total time of reaction with steam was 10 min. During the first 8 min, the fuel element was being elevated into the high-temperature section. The fuel element was kept in the high-temperature section for 2 min and was then rapidly withdrawn to the original position in the cooler part of the furnace.

The typical appearance of a fuel element which was exposed to steam under these conditions is shown together with an unexposed element in Figure 22. The temperature-time history of the top (hottest) end of the fuel element is given in Figure 23 together with a plot of the hydrogen evolution. The top of the fuel element reached a maximum temperature of about 1600°C, and the bottom a maximum of about 900°C, thereby creating an axial temperature gradient of about 700°C. The top one-third of the stainless steel cladding appeared to be completely reacted, whereas the remainder had reacted only slightly. The demarcation between the two

reaction zones can be readily seen in Figure 22. The maximum temperature at the demarcation has been estimated to be 1400°C from the results of other experiments.[23] The total hydrogen evolved corresponded to 47% reaction of the stainless steel present in the fuel element.

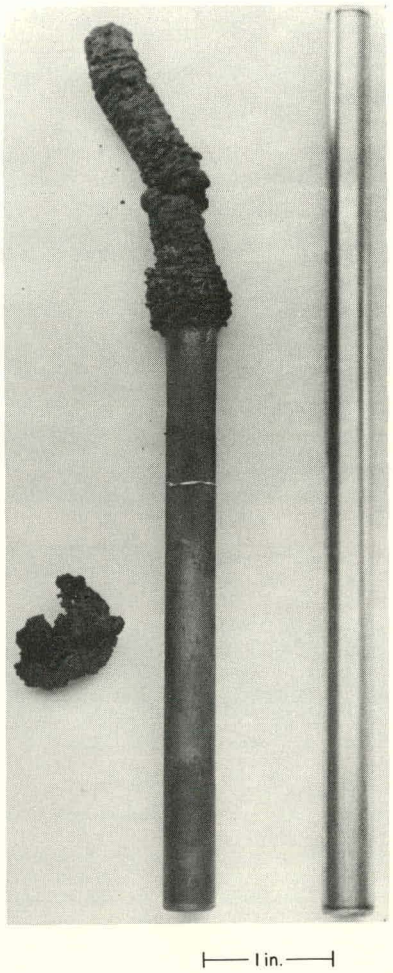

Figure 22

304 Stainless Steel-clad, UO_2 Core Simulated Fuel Pin Before and After Exposure to One atm Steam at 1600°C for 10 min

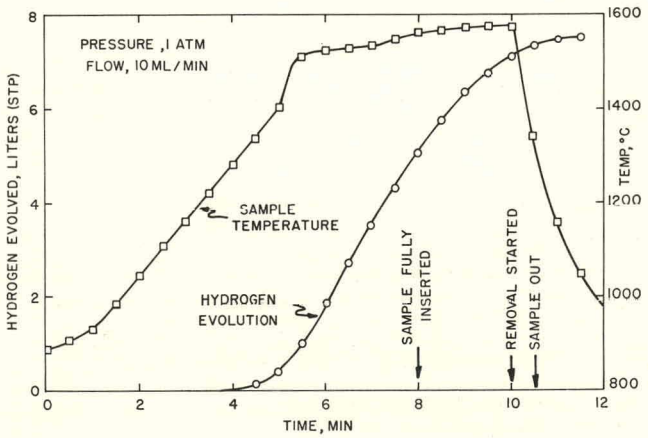

Figure 23. Hydrogen Evolution and Sample Temperature During Stainless Steel-304-clad Fuel Rod Experiment in High-pressure Furnace

[23] Chemical Engineering Division Semiannual Report, January-June 1964, ANL-6900, p. 239.

A photomicrograph of a radial cross section near the top of the fuel element (see Figure 24) showed areas of interaction between the UO_2 and the stainless steel oxides. The foamy appearance of the oxidized stainless steel is also apparent in the photomicrograph. X-ray analysis of the stainless steel oxides showed a structure of the γ-Fe_3O_4 type.

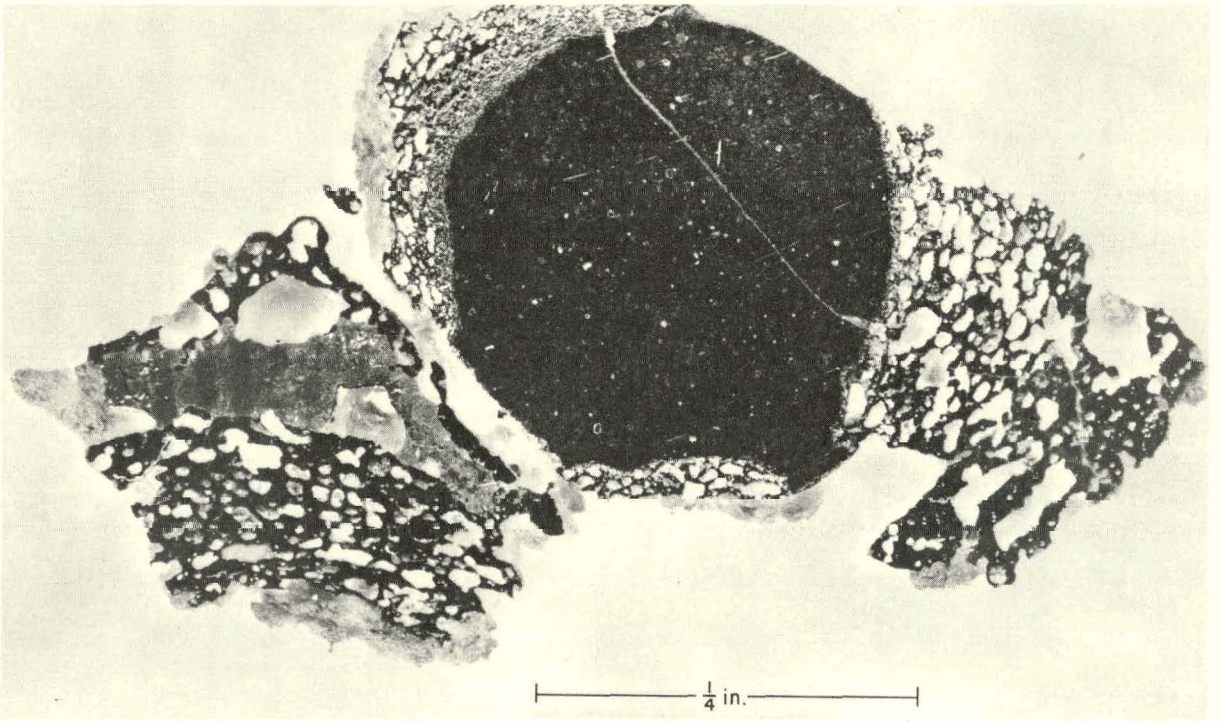

Figure 24. Radial Cross Section Near the Top of a 304 Stainless Steel-clad, UO_2 Core Simulated Fuel Pin Exposed to One atm Steam at 1600°C for 10 min

Additional experiments were conducted to determine the effects of both steam flow rate and steam pressure. In the first of these experiments, the pressure was maintained at 1 atm and the steam flow rate was increased to 20 ml/min of water. In the second and third experiments, the steam flow rate was maintained at 10 ml/min of water and the pressure was increased to 4 and 11 atm. Neither the rate nor the extent of stainless steel-steam reaction were significantly affected by the changes in steam flow rate or pressure.

c. Reaction of Zircaloy-2-clad Fuel Elements with Steam. A preliminary experiment with a Zircaloy-2-clad fuel element was described in the Progress Report for December 1964, ANL-6997, p. 57. The conditions of the experiment were identical with those of the first experiment with the stainless steel-clad fuel element, i.e., low steam flow rate and long residence time (see Section IV.C.1.b). The upper two-thirds of the Zircaloy-2 cladding appeared to be reacted completely, forming a tube of ZrO_2 which retained the original shape of the metal cladding. The lower

(cooler) portion of the cladding reacted only slightly. Most of the reaction occurred during the first 2 hr of the exposure. Again, it was apparent that the low steam flow rate had limited the rate of reaction.

Additional experiments with Zircaloy-2-clad fuel elements were performed with an increased steam flow rate of 10 ml/min of water and the shortened residence time described in Section IV.C.1.b in connection with the stainless steel-clad elements.

The typical appearance of a Zircaloy-2-clad fuel element which was exposed to steam under these conditions is shown together with an unexposed element in Figure 25. The temperature-time history of the top (hottest) end of the element is given in Figure 26 together with a plot of the hydrogen evolution. The top and the bottom of the fuel element reached maximum temperatures of 1600 and about 900°C, respectively, resulting again in an axial temperature gradient of about 700°C. The hot upper end of the sample was embrittled, and only the outer surface was converted to ZrO_2. There was no apparent interaction between the UO_2 and the cladding. In the case of Zircaloy-2-clad fuel pin, there was no sharp demarcation between reaction zones; however, the attack on the cladding was more severe at the hotter end than at the cooler end.

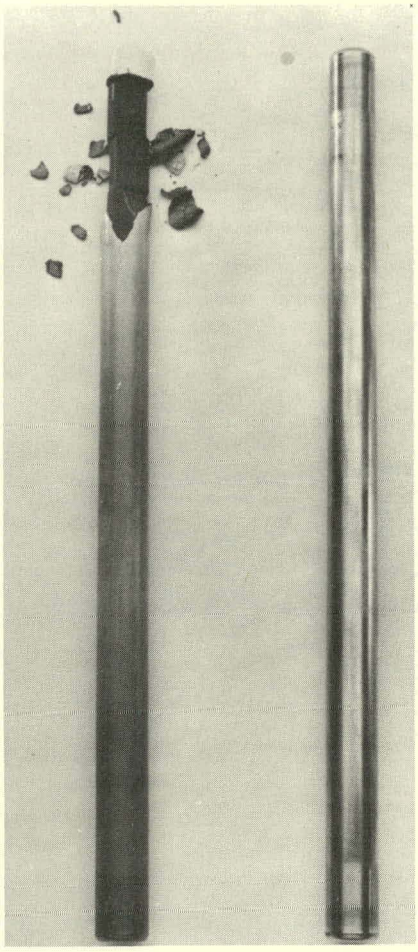

Figure 25

Zircaloy-2-clad, UO_2 Core Simulated Fuel Rod Before and After Exposure to One atm Steam at 1600°C for 10 min

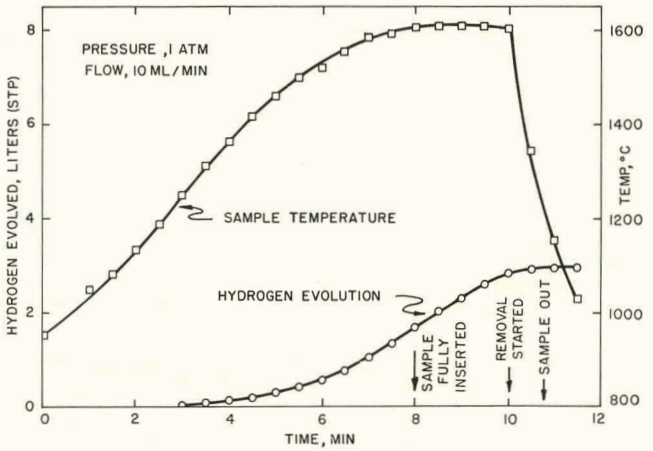

Figure 26. Hydrogen Evolution and Sample Temperature During Zircaloy-2-clad Fuel Rod Experiment in High-pressure Furnace

Figure 27 shows a cross section of the top cap of the fuel pin. Measurements made on the photomacrograph indicated that a layer of tubing wall, 14 mils thick, remained as metal (original thickness, 27 mils). Measurement of the evolved hydrogen indicated that the overall extent of reaction of Zircaloy-2 in the fuel element was 18%.

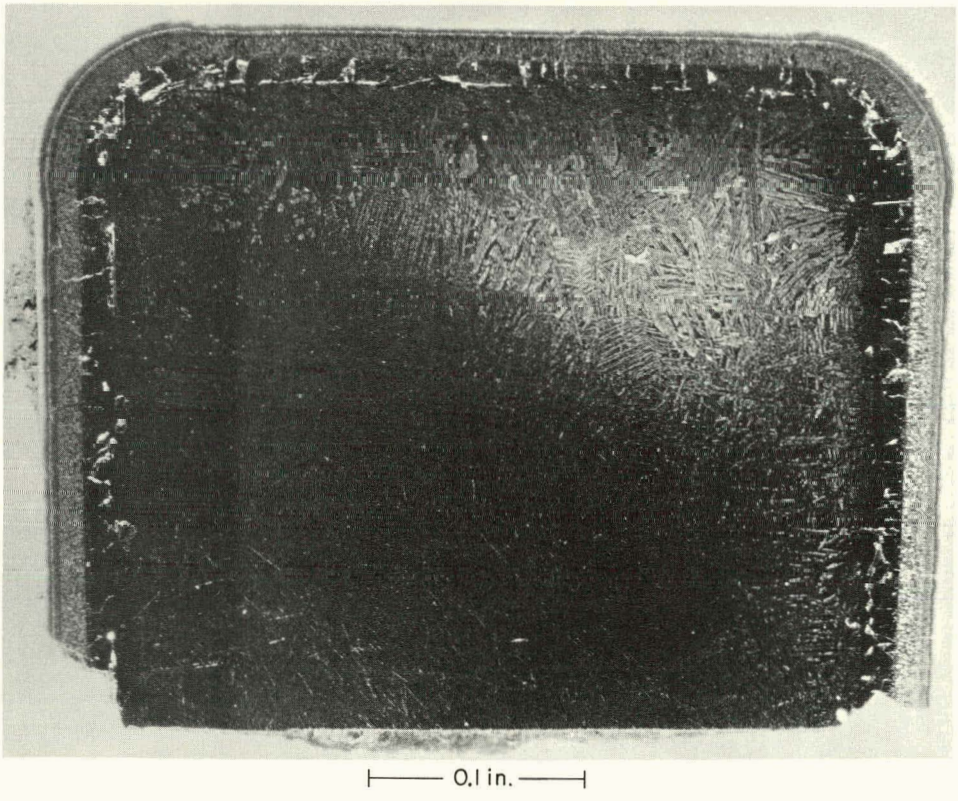

Figure 27. Cross Section of the Top Cap of a Zircaloy-2-clad, UO_2 Core Simulated Fuel Pin After Exposure to One atm Steam at 1600°C for 10 min

A parabolic oxidation law was used to calculate the extent of reaction at the hotter end of the fuel element. The calculations indicated that 14 mils of the Zircaloy should react with the steam; this is in close agreement with the value calculated from measurements made on the photomacrograph.

Experiments with Zircaloy-2-clad fuel elements were also performed at pressures of 4 atm and 11 atm. As in the case of the experiments with stainless steel (see Section IV.C.1.b) there was no significant effect of pressure on either the rate or the extent of the Zircaloy-2 steam reaction.

d. Comparison of the Stainless Steel-Steam Reaction with the Zircaloy-2-Steam Reaction. The results of the experiments with stainless steel-clad and Zircaloy-2-clad fuel elements (see Sections IV.C.1.b and IV.C.1.c) indicate that above 1400°C the reaction of stainless steel with steam is more rapid than that of Zircaloy-2 with steam. The rapidity of the stainless steel reaction under these conditions is due to the melting and foaming (and the subsequent large increase in surface area) of the mixture of stainless steel and stainless steel oxides. The rapidity of the oxidation of the stainless steel as it reaches about 1400°C results in observable self-heating of the cladding, as indicated in the temperature-time history in Figure 23. Neither Zircaloy nor ZrO_2 are melted under the conditions of these experiments. However, the overall heat of reaction of Zircaloy with steam is much greater than the heat of reaction of stainless steel with steam.

Calculations presented in a recent analysis of a loss-of-coolant accident in a reactor which utilizes zirconium-clad fuel have indicated that the reaction at temperatures greater than 1000°C will probably be limited by the availability of steam to the reactor core.[24] These calculations were performed using the parabolic oxidation law for the zirconium-steam reaction. A rate law for the stainless steel-steam reaction has not yet been established because of the spontaneous disintegration of stainless steel at 1400°C, which results in a changing surface area. The sharp increase in reaction rate resulting from the increased surface area suggests that similar reactor calculations can be performed for stainless steel-clad fuel using the approximation that the reaction rate is negligible below 1400°C and limited by the availability of steam above 1400°C.

---

[24]Baker, L., Jr., and Ivins, R. O., Nucleonics 23 (7), 70 (1965).

V. PUBLICATIONS

Papers

OXIDATION-FLUORINATION OF URANIUM DIOXIDE PELLETS IN A FLUIDIZED BED

L. J. Anastasia and W. J. Mecham

Ind. Eng. Chem. Process Design and Development 4(3), 338-344 (July 1965)

ANALYZING THE EFFECTS OF A ZIRCONIUM-WATER REACTION

Louis Baker and R. O. Ivins

Nucleonics 23(7), 70-74 (July 1965)

FLUORINE BOMB CALORIMETRY. X. THE ENTHALPIES OF FORMATION OF NIOBIUM AND TANTALUM PENTAFLUORIDES

Elliott Greenberg, C. A. Natke, and W. N. Hubbard

J. Phys. Chem. 69, 2089-2093 (June 1965).

FLUORINE BOMB CALORIMETRY. XI. THE ENTHALPY OF FORMATION OF YTTRIUM TRIFLUORIDE

Edgars Rudzitis, H. M. Feder, and W. N. Hubbard

J. Phys. Chem. 69, 2305-2307 (July 1965)

FLUORINE BOMB CALORIMETRY. XII. THE ENTHALPY OF FORMATION OF RUTHENIUM PENTAFLUORIDE

H. A. Porte, Elliott Greenberg, and W. N. Hubbard

J. Phys. Chem. 69, 2308-2310 (July 1965)

Pu-Cd SYSTEM: THERMODYNAMICS AND PARTIAL PHASE DIAGRAM

Irving Johnson, M. G. Chasanov, and R. M. Yonco

Trans. Met. Soc. AIME 233, 1408-1414 (July 1965)

REACTION OF FLOWING STEAM WITH THE REFRACTORY METALS NIOBIUM AND TANTALUM

Martin Kilpatrick and S. K. Lott

J. Less-Common Metals 8, 299-305 (May 1965)

DISTRIBUTION OF TRANSURANIUM ELEMENTS BETWEEN MAGNESIUM CHLORIDE AND ZINC-MAGNESIUM ALLOY

J. B. Knighton and R. K. Steunenberg

J. Inorg. Nucl. Chem. 27, 1457-1462 (1965)

THE BOILING LIQUID METAL PROGRAM AT ARGONNE NATIONAL LABORATORY

R. C. Brubaker, J. B. Heineman, R. E. Holtz, and R. P. Stein

Proc. 2nd Joint USAEC-EURATOM Two-Phase Flow Meeting held at Germantown, Md., April 29-May 1, 1964, ed. R. M. Scroggins. CONF-640507 (Nov 1964), p. 3.1.1

BUILDING 11 TWO-PHASE FLOW PROGRAM
Michael Petrick
Proc. 2nd Joint USAEC-EURATOM Two-Phase Flow Meeting held at Germantown, Md., April 29-May 1, 1964, ed. R. M. Scroggins. CONF-640507 (Nov 1964), p. 6.5.1

FOG FLOW MODELS
R. P. Stein
Proc. 2nd Joint USAEC-EURATOM Two-Phase Flow Meeting held at Germantown, Md., April 29-May 1, 1964, ed. R. M. Scroggins. CONF-640507 (Nov 1964), p. 6.1.1

FAST REACTOR PHYSICS PARAMETERS FROM A PULSED SOURCE
W. Y. Kato, H. H. Meister, G. W. Main, J. L. Russell, and K. Crosbie
IAEA Symp. on Pulsed Neutron Research, Karlsruhe, Germany, May 10-14, 1965. Abstracts of Papers SM-62/56

BREEDER REACTORS--TOMORROW'S POWER PLANTS
J. T. Madell
Ind. Res. 7(8), 58-63 (July 1965)

TABLE ERRATA
H. C. Thacher
Math. Comp. 19(91), 527 (July 1965)

The following appeared as Abstracts in Trans. Am. Nucl. Soc. 8(Suppl.) (1965):

RECENT PROBLEMS WITH EBR-II COMPONENTS
G. K. Whitham and J. D. Leman
pp. 11-12

IDAHO DIVISION REACTOR OPERATIONS PERSONNEL TRAINING PROGRAM
Harry Bryant
pp. 15-16

PLANT SYSTEMS TRAINING OF PERSONNEL FOR EBR-II
C. L. Nelson, G. K. Whitham, Harry Bryant, J. D. Leman, and J. K. Greene
p. 16

DEFECTIVE FUEL TESTS IN THE NUCLEAR SUPERHEATING REACTOR BORAX-V
D. C. Cutforth, C. C. Miles, and Robert Villarreal
pp. 35-36

EBR-II REACTOR BUILDING LEAK TESTING
G. K. Whitham, F. J. Tebo, and F. D. McGinnis
pp. 40-41

ANL Report

ANL-6995 THE MANUFACTURE OF GLASS-BONDED FUELS FOR DOPPLER COEFFICIENT MEASUREMENT
J. E. Ayer, A. G. Hins, D. E. White, D. C. Carpenter, and C. F. Konicek